February 25, 2000
OSGCP Project No. R/OE- (14)
Project Duration: Mar. 1, 1998 to Feb. 29, 2000

DEVELOPMENT OF A MICROPROCESSOR-BASED JOINT TRACKING AND OPERATION GUIDANCE SYSTEM FOR UNDERWATER WELDING

Final Report

Submitted to

Ohio Sea Grant College Program

The Ohio State University

1314 Kinnear Road

Columbus, Ohio 43212-1194

Submitted by

Chon L. Tsai, Baojian Liao, David A. Clukey, Joseph S. Breeding

Department of Industry, Welding and Systems Engineering

The Ohio State University

EXECUTIVE SUMMARY

A series of research projects applying flux-cored welding process to underwater "wet" welding have been conducted by the investigator, Professor Chon Tsai and his underwater welding group at The Ohio State University. A contoured shroud corresponding to the critical welding zone was developed for protection of the arc, weld pool and heat affected zone. A bubble-status monitoring and feedback control algorithm was also developed. These developments enable the arc to burn smoothly in a stable gas bubble while protecting the weld area from the water environment to slow down the cooling rate of the weld. The results of these projects show significantly improved arc stability and weld appearance. Analysis of microstructures and mechanical properties show that satisfactory underwater welds could be made with 308L flux-core wire on A36 mild steel using this method if the welding operation is carefully controlled so that the welds are deposited correctly to fill the joints.

A major difficulty in underwater welding operations is poor visibility both of the position of the joint and of the weld pool conditions. The causes of the poor visibility include image distortion by the moving bubble-water interference, muddy water, fumes from welding, and, for flux-cored welding, the shroud. This project was initiated to improve the operational maneuverability and further increase weld quality by providing a visual signal of the joint center position for the diver/welder, or by use of a mechanized, feedback controlled seam-tracking system. The welding arc itself was utilized as the sensor to detect the arc-joint position deviation. This error was converted to visual signals and displayed in the diving helmet to give the diver/welder guidance. In the mechanized system, with feedback control logic, an actuator was used to adjust the position of the welding torch to track the center of the joint. A high-speed-spinning arc sensor, which has the arc circularly scanning the joint at a frequency of 20~30Hz, was adopted in the project. A PC-based control system was first setup to sample and process the arc current signals, develop the control logic and gather data for establish a reference database. Then

a microcontroller-based prototype for future commercial design was developed. The control program was coded in EEPROM (electrical programmable read-only-memory). This single board circuit has integrated all the required functions: data acquisition, processing, feedback control and visual signal display control. This unit not only is more compact, less costly than a PC system, but it also provides higher working reliability in industrial environments.

Theoretical derivation was performed to setup arc sensor models and analyze the characteristics with respect to the spinning frequency. Experiments were conducted to verify the models, find the model parameters, select and optimize control parameters, and to compare in-air and underwater welding arc sensors. Both fully mechanized, automatic feedback seam tracking welding and manual semi-automatic welding tests were performed.

Both the PC-based experimental system and the microcontroller-based commercial prototype have successfully performed feedback joint tracking in the test tank with mechanized system. Following the guidance provided by the visual signals, it is also possible for the operator to manually track the joint. The microcontroller-based prototype has been successfully integrated and refined. With this tracking system and the contoured shroud developed in previous research, welds with good bead profiles, sound microstructures and mechanical properties were produced in underwater wet welding.

ACKNOWLEDGMENTS

The author would like to acknowledge and thank the many people who contributed either their time, financial resources, or both. Special thanks and recognition go to Dr. Jeffrey M. Reutter, Director of the Ohio Sea Grant College Program for his generous and continuing support of the underwater welding projects at The Ohio State University. His support has been instrumental to the success of many projects.

Generous support has been received from The Welding Consultants Inc. (William Svekric, President), with both financial and material resource contributions.

Special thanks to Ravi Menon from Stoody company for supplying the 308L flux-cored wire used in our research and for his continuing support of this and related projects.

TABLE OF CONTENTS

LIST OF TABLES

LIST OF FIGURES

CHAPTER 1

INTRODUCTION

1.1 Background

Underwater "wet" welding has been limited in use because of the known difficulties associated with exposing the weldment to the water environment (Brown et al. 1974, Masubuchi et al. and Stalker et al. 1975, Grubbs et al. 1976, Tsai et al. 1977, 1979, 1985, Gooch 1983, Dexter et al. and Cochrane et al. 1986, Matlock et al. and Dally et al. 1987). Recent investigations into the underlying problems of "wet" welding have yielded much greater insight into these difficulties allowing the development of superior welding electrodes, procedures, equipment and techniques which mitigate many of the problems and reduce the impact of others on the serviceability of "wet" welds (Ibarra et al. 1989, 1993, West et al., Ogden et al. and Oh et al. 1990, Tsai et al. 1991, 1992, 1994, 1995, Sanchez-Osio et al. and Grubbs et al. 1993). These developments and investigations have more fully defined the chemical, metallurgical and mechanical properties of "wet" welds and have pointed the way for development of even better weld properties. Along with the welding investigations, innovative design concepts have been developed and tested that circumvent some of the "wet" welding problems and can be used to assure satisfactory weld performance (Tsai et al. 1989, 1990, 1991, 1994, Waston et al. 1994). When coupled together, the improved material properties and improved design concepts can be utilized to produce "wet" welding repairs and modifications to underwater structures and pipeline systems that are fit-for-service (Tsai et al. 1995).

Since 1985, the authors have conducted a series of research programs to efficiently use underwater "wet" welding for various industrial applications. These research programs, either individually sponsored or co-sponsored by the Ohio Sea Grant College Program, The Thomas Edison Program of the State of Ohio, National Coastal Resources Research and Development Institute, US Navy Joining Center and two Ohio companies, have resulted in the development of a fitness-for-service design solution, including a new design methodology and an improved

underwater "wet" welding electrode. This design approach can fulfill underwater structural requirements using the existing underwater "wet" welding technology.

As part of a parallel effort, the authors have conducted research on underwater Flux-Cored Arc Welding (FCAW) since 1994. FCAW is a semiautomatic welding process that can continuously operate until completion of a weld pass. Unlike the Shielded Manual Arc Welding (SMAW) process, which requires changing electrodes from time to time, the FCAW arc is normally uninterrupted during a welding pass. This reduces weld cracking sensitivity, especially for those steels with carbon equivalent content higher than 0.4%, by avoiding the severe water quenching of the weldment at the point of arc extinguishment and re-ignition. A further major advantage of the FCAW process is its good adaptability for mechanization or even automation in an underwater environment.

The technology of the FCAW process has been developed to become an alternative to the SMAW process for underwater wet welding. A smart underwater welding process control algorithm was developed. Weld quality was significantly improved by a new arc bubble control and the welding zone shielding method. A contoured shroud covering the weld surface and the critical heat flow zone can effectively improve the arc stability, protect the welding pool, reduce the hardness in the weld and heat-affected-zone, and eliminate many arc starts and stops during welding. These improvements result in more consistent weld quality, with less dependency upon the welding skills of the welder and on the environment conditions, and also result in the best welding performance. An analysis of microstructures and mechanical properties showed that satisfactory underwater welds could be made using 308L flux-cored wire on A36 mild steel. The welding operation must be controlled so that the welds are deposited correctly to fill the joints.

A major deterrence to adopt the FCAW process for underwater wet welding is the difficulty in tracking the joint precisely, especially when welding in muddy water or under the condition of poor visibility or poor joint accessibility. These circumstances are often encountered when repair work is performed in a lake or river. The greatest challenge to underwater wet FCAW process is to be able to move the arc along the joint in locations of poor visibility, restricted maneuverability, or inaccessible corners.

Another challenge to the process is to adjust the welding parameters appropriately according to the joint conditions during welding. The diver/welder has no information regarding the frequent changes in welding current and voltage due the inability to hear the arc sound or view the arc plasma in the underwater environment.

Machine vision could be a solution to the underwater visibility problem. The authors have studied the application of a miniature waterproof camera and fiber optics in underwater welding (sponsored by National Coast Research and Development Institute). With this system the video signal from the camera of the welding zone was delivered to an eyepiece video monitor mounted in the diving helmet, providing the welder with information about the joint position and the weld condition. The difficulty of this method is that optical and electronic devices are vulnerable to the arc and water damage. The arc light, welding fume, spatter, and bubble-water interface inference may degrade the image quality severely. Special protection and a larger distance from the arc are required. The vision system is better used to monitor a larger area of the welding structure, rather than to focus on the weld arc.

Through-arc seam tracking could be a good solution to this problem. This method uses the arc itself as the sensor to detect the torch-joint deviation. Therefore, it is not interfered with the harsh arc and water environments, as long as the welding process is stable. The authors have developed an innovative joint tracking system with high-speed spinning arc sensor for in-air welding conditions in earlier research. The spinning arc joint tracking technique uses a rotary encoder and a current sensor that can continuously monitor the current waveform and the arc position. For a given joint detail, the current waveform detected from the spinning arc will show a specific pattern and relationship with the joint geometry. These pattern and relationship can be used to determine the instantaneous location of the torch center in a joint during welding.

1.2 Objectives

The objective of this proposed study is to develop an intelligent system to assist diver/welder in performing the underwater "wet" flux-cored arc welding (FCAW) process in an environment of poor visibility, restricted maneuverability, and limited accessibility. A spinning arc sensor for joint tracking will be integrated into a microprocessor-based information system to provide the diver/welder with guidance during manually operated welding, and to automatically adjust the torch position to track the joint center in mechanized welding. A microprocessor-based unit will be used for data acquisition, processing and control. Sensors will be used to monitor the real-time arc spinning position, current waveform, arc voltage, as well as other parameters

indicating arc and gas bubble state. These signals will be processed against the programmed database and generate a real-time instruction for manual welding controlled by the diver/welder. The information will be displayed as visual signals on a display device and/or audio signals with an audio device embedded in the diving helmet. In a mechanized welding system, through a feedback control algorithm, the information is also used to drive an actuator to adjust the torch position to correct the torch-joint deviation. The intelligent system is to circumvent the difficulties associated with the FCAW process in underwater wet welding.

1.3 Impacts/Benefits

Underwater "wet" welding has been used successfully for repair of marine structures and, to a limited extent, for original construction. The microprocessor-based joint tracking system and the intelligence built into the flux-cored arc welding system will circumvent the difficulties due to poor visibility, limited joint accessibility, and restricted maneuverability under many adverse underwater conditions. This new welding process will enhance wet weld reliability. More permanent underwater welding repairs or even construction using wet welding technology may become reality. This will result in further expansion of human activities into more difficult underwater environments, a more competitive shipping industry, or safer nuclear energy utilization.

The intelligent, underwater flux-cored arc welding process with joint tracking ability by a spinning arc will enhance the capability of engineers to perform semi-automatic and automatic underwater wet welding in an environment with virtually no visibility. The success of this projectmay allow the use of remote operated vehicles, deep water applications, welding of other material groups that are presently difficult to weld with the shielded metal-arc welding (SMAW) process.

The significance of offshore, coastal, inland waterway, big lake and port facilities to the economic survival of a given region, the ability to cope with all aspects relative to safety and damage due to hurricanes and earthquakes and their resulting storm surges and possible tsunamis has become a pressing responsibility of the engineering profession. Underwater wet welding is an important and efficient technique to restore damaged structures. Recent advancements in wet welding technology enhance the ability of mitigating structure damage with fast response at reasonable costs.

Other industrial sectors that could be benefited by such a technological advancement include shipping industries and nuclear power plants. Damaged ship structures under the

waterline can be repaired using underwater "wet" welding without dry-docking. The submerged nuclear reactor components have also been repaired underwater at much reduced cost in comparison to dewatering and repair process. With many of the nuclear power plants worldwide reaching their design life, reliable and efficient restoration techniques become urgent. This urgency for improved underwater wet welding technology has been growing at an unprecedented rate as new aging problems occur every day. The same benefits in assuring public safety and efficient utilization of resources can be appreciated by the power utility industry.

1.4 Methodology

The intelligent sensing and operational guidance system developed in this project consists of four basic elements: (1) spinning arc mechanism and servo control, (2) welding parameters and arc positioning sensors, (3) decision reference architecture and microprocessor control unit, (4) display unit integration for information delivery in manual welding, and electronically controlled torch position adjusting actuator in automatic welding.

The FCAW system uses a constant voltage output power supply and the newly developed contoured shroud. Type 308L stainless steel self-shielding flux-cored welding wire was used. The spinning arc joint tracking component was developed first. A servomotor driven mechanism spins the electrode contact tip, which causes the arc to sweep across the joint in a circular motion during welding. The continuous changes in welding current while the arc is sweeping across the joint are detected with a current sensor. This electric current waveform has a definite relationship to the horizontal and vertical distance deviations between the contact tip and the joint surfaces. The momentary location of the arc with respect to the joint geometry can therefore be determined by analyzing the current waveform and its geometry relationship.

According to results of earlier research on in-air welding, a higher sweeping frequency will improve traverse sensing gain and dynamic response. But some differences could be expected between underwater arc and in-air arc behaviors. The underwater arc sensor characteristics were studied, by mathematical analysis, simulation and experiments, to obtain the necessary knowledge for selecting spinning frequency and determining the pattern recognition algorithm.

The current waveform was processed and analyzed in both time and frequency domains. The mode recognition technique in reference to the arc sensor model will be used to obtain real-time information about the contact tip to workpiece distance, the horizontal deviation and the joint surface contour. The original current waveform and the deduced reference joint pattern were

transferred to a visual graphic display to guide the diver/welder in adjusting the torch position. Electrical signals were interfaced with the driving circuit to automatically adjust the torch position in the mechanized joint tracking system,

A prototype system with a desktop PC as control unit was developed first. This system includes a PC, a board with A/D and D/A converters, digital I/O ports, and signal conditioners for noise isolation and signal amplification. An integration software program was developed to perform real-time acquisition and processing of arc parameters, control algorithm and converting them into visual output signals. Experimental tests were conducted to establish correlation among the significant process variables including spinning frequency, sweeping range, mean current, sensor gains, and their relationships with the resulting weld quality. The correlation was developed specifically to fit the underwater welding arc characteristics.

Once the prototype sensing and operation guidance system was optimized, various components were integrated into a microcontroller-based commercial demo system. The microcontroller chip was integrated together with the sensors, data acquisition hardware and software, and visual delivery media into a welding and diving system. The visual devices were attached to a welding helmet. The diver/welder can operate the welding torch according to the instructions provided by the control system. The commercial demo system was tested in underwater conditions and refined for accuracy, fast response and ease of use. Compared to the PC system, the microcontroller system is more suitable for industrial field application due to its small size, lower cost and high ability to resist electronic interference. It can be used as the product design model.

CHAPTER 2

MODELS OF JOINT TRACKING WITH SPINNING ARC SENSOR

2.1 Introduction to Seam Tracking with Arc Sensor

Although what is emphasized in this report is underwater welding visibility and joint tracking, seam tracking has been one of the most important problems in arc welding automation in the surface environment. Reliable, precise and real-time detecting of the deviation of torch to groove center is the basis of seam tracking.

Seam tracking with arc sensor (or Through Arc Seam Tracking) has been used in industry for some time. Most new arc welding robots are equipped with arc sensor for seam tracking and are successfully used in many applications. This technique uses the arc itself as the sensor to make the system more robust than with other sensors. With no extra sensing component at the tool tip, the accessibility is close to a regular torch.

Using arc parameters to detect the torch to joint deviation eliminates the difficulties caused by disturbance of the harsh welding environment to electrical, magnetic or optical sensors. This makes the tracking system more reliable. Through arc seam tracking was considered an economical yet effective method of welding joint tracking.

Welding seam tracking by arc sensor is based on the arc length change. In Gas Tungsten Arc Welding (GTAW), which uses constant-current characteristic power supply, the arc voltage changes with the arc length change. Thus arc voltage signal is used to detect the arc length. When sweeping the torch across the groove, the voltage changes according to the groove surface contour, therefore, the related transversal position of the joint to the torch can be found. In the Gas Metal Arc Welding (GMAW) and Flux-cored Arc Welding (FCAW) processes, which use constant voltage characteristic power sources, the welding current, instead of voltage, changes according to the change in the conduct tip workpiece distance (CTWD) change. Current commercial systems equipped on robots usually realize lateral sensing by weaving the robot arm to make the arc scan over the joint groove. By comparing the currents at the left and right

extremity, the deviation of the joint line center and torch nominal center can be determined. Then with feedback control logic the torch position can be adjusted against the programmed route.

The arc parameters (current and voltage) are related to welding process, electrodes and plasma properties, anode-cathode distance, wire feeding, and welding power supply characteristics. Despite the wide use of through arc seam tracking, the systematical description on arc sensor system control model, especially the dynamic characteristics, is still under development.

In this chapter, the static and dynamic arc sensor models are analyzed based on physical-mathematics derivation and simulation, then verified with experiments. Some of the results are based on the earlier research of the authors. This analysis will give a better understanding of arc sensor systems, and the relationship between the many factors involved in GMAW or FCAW process. Both in-air welding and underwater welding were performed to compare the differences. One of the important and most useful results is the higher sensitivity of the arc sensor at higher scanning frequency.

2.2 Static Model of Arc Sensor

The static model describes the relationships between average arc current and contact-tip-to-work distance (CTWD) when the welding is in steady state, that is, at the state of fixed CTWD, wire feed rate, power source setting, and the arc is stable.

2.2.1 Theoretical Derivation

The static model of arc sensor can be derived from the relations among the CTWD, H and average arc current I, arc length L_a, and feed wire stick out (from the contact tip to arc) length L_s, when the arc is at steady state. Many researchers have reported their work on some parts of this system.

In gas shielded metal arc welding (GMAW, FCAW), usually constant voltage (CV) power source and constant wire feeding rate is adopted. The system is shown in Figure 2.1.

Equation (2.1) can describe the output characteristics of the power supply at the working point:

$$U = U_{ol} - R_s I \tag{2.1}$$

Where U_{ol} is the equivalent open loop voltage, and R_s is the dropping slope (equivalent source resistance, include the welding cables).

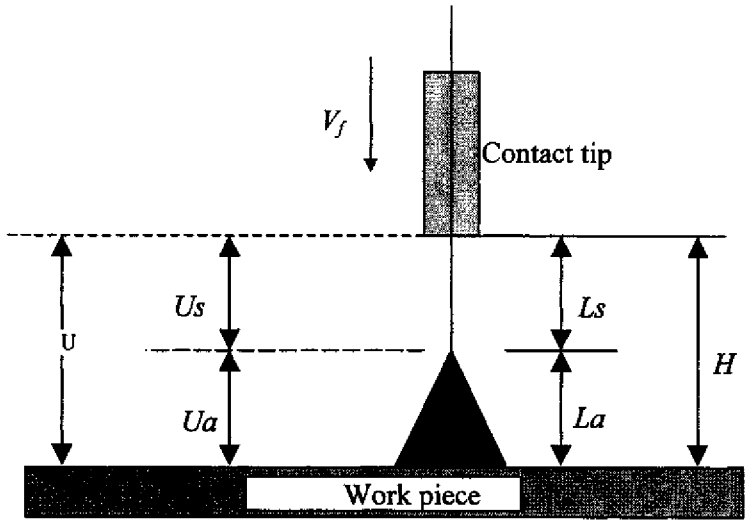

Fig. 2.1 Illustration of arc parameters

The power output voltage is distributed in two parts: arc voltage U_a and the wire stickout voltage U_s:

$$U = U_a + U_s \tag{2.2}$$

GMAW and FCAW arc voltage-current characteristics can be described as Equation 2.3:

$$U_a = K_a L_a + R_a I + U_c \tag{2.3}$$

Where K_a is electrical field intensity, that is voltage drop of unit length of arc column. R_a is the slope resistance of arc. U_c is a constant related to anode and cathode voltages.

The voltage dropped on the wire stickout is equal to its electric resistance multiplied by the arc current:

$$U_s = \rho \frac{L_s}{A} = K_s L_s I \tag{2.4}$$

Where ρ is the average electric resistivity of the wire over the temperature ranges. A is the electrode (wire) cross-section area. K_s is the average resistance of unit length of stickout wire.

The wire melting rate, according to Lesnewich and Halmoy, can be described as:

$$V_m = K_m I + K_e L_s I^2 \tag{2.5}$$

Where V_m is the melting rate; $K_m I$ is the melting rate from the arc heat; K_m is the constant related to anode voltage drop. $K_e L_s I^2$ is the stickout wire resistance heat contribution to melting rate; K_e is another constant. These constants are determined by wire melting heat and efficiency factors. In steady state, the melting rate, if represented in wire length per unit time, equals to wire feed rate:

$$V_m = V_f \tag{2.6}$$

Finally, the contact–tip-to-workpiece distance is composed of the arc length and stickout length:

$$H = L_s + L_a \tag{2.7}$$

In these seven equations, when welding process given, power source voltage, possibly drop slope, CTWD and wire feed rate are controllable parameters. Arc length and current are the most concerned output parameters. The *H-I* relationship is the arc sensor model, which is used for arc sensor design. Other factors, such as shielding gas type or wire type will show their effects by the coefficients or constants in equations.

Now derive *H-I* relationship. From Equ. 2.5 and Equ. 2.6, we can get:

$$L_s = \frac{V_f}{K_e I^2} - \frac{K_m}{K_e I} \tag{2.8}$$

Substituting this result into the other equations, *H-I* relation can be found as the following equation:

$$\begin{aligned} H &= \left(\frac{U_{ol} - U_c}{K_a} + \frac{K_s K_m}{K_a K_e}\right) - \left(\frac{R_s + R_a}{K_a}\right) I - \left(\frac{K_s}{K_a K_e} V_f + \frac{K_m}{K_e}\right) \frac{1}{I} + \frac{1}{K_e} V_f \frac{1}{I^2} \\ &= K_1 - K_2 I - K_3 \frac{1}{I} - K_4 V_f \frac{1}{I} + K_5 V_f \frac{1}{I^2} \end{aligned} \tag{2.9}$$

It can be linearized by Taylor's expansion at a setting point I_0. The experimental results in the next subsection show that in the normal welding parameter range, the linearity is very good. The equation is:

$$H = (a_1 V_f + b_1) - (a_2 V_f + b_2) I \tag{2.10}$$

Where a_1, a_2, b_1, b_2 are derived constants.

$$a_1 = \frac{3}{K_e I_0^2} - \frac{2K_s}{K_a K_e I_0}$$

$$b_1 = \frac{U_{ol} - Uc}{K_a} + \frac{K_s K_m}{K_a K_e} - \frac{2K_m}{K_e I_0}$$

$$a_2 = \frac{2}{K_e I_0^3} - \frac{K_s}{K_a K_e I_0^2}$$

$$b_2 = \frac{R_s + R_a}{K_a} - \frac{K_m}{K_e I_0^2}$$

The static sensitivity of arc sensor, that is the current change cause by unit CTWD change, is:

$$S_{st} = | dI / dH | = 1 /(a_2 V_f + b_2)$$

Its unit is A/mm.

2.2.2 Experiment Test on Static Arc Sensor Characteristics

Table 2.1 Arc current at different contact-to-work-distance

CTWD: H		Arc Current: I
Inch	mm	(Ampere)
1	25.4	154
7/8	22.2	160
3/4	19.0	166
5/8	15.9	174

Experiments were performed to verify the relation between arc current and CTWD. Table 2.1 and Figure 2.2 show the experimental results under the following conditions:

Underwater welding water depth: 250mm (10inch); Wire type: 308L; Feed rate: 5.1m/mm (200ipm); Voltage: 29V, no external applied shielding gas.

The regressed equation of this set of data is:

I=206.4-2.08H

Where I in Amperes and H in millimeters. The linearity is very good as shown by the correlation coefficient R^2=0.9945.

The sensitivity is: S_{st} = 2.08A/mm.

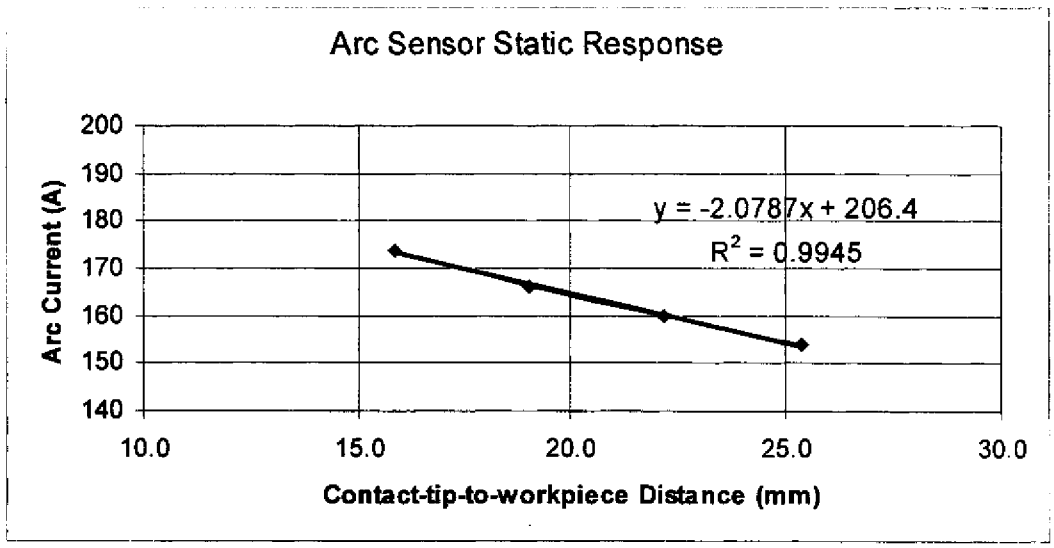

Figure. 2.2 Arc sensor static response

2.3 Dynamic Model of Arc Sensor

2.3.1 Theoretical Analysis

In welding practice, it can be observed that when CTWD increases some length abruptly, the "soft" arc will stretch at the same increased length but will shorten later and reached a new steady state. The dynamic model of the arc-power system describes such transient characteristics when one or more parameters change. The arc sensor frequency response (sensitivity at different frequencies) will be of most concern.

The dynamic arc sensor model is based on the same equations used in static model deviation, but take their dynamic types (differential equations). With perturbation model (considering small change around a set point) and reasonable linearization, the equations are discussed in frequency domain with their Fourier transformed types.

In the following discussion of the dynamic model, lowercase symbols represent the instantaneous value of the parameters; uppercase symbols with the augment (s) represent the Fourier Transforms of the perturbations of the corresponding parameters; uppercase symbols without the augment (s) represent the perturbations of the parameters to their set points, and the suppressed form of their Fourier Transforms. For example, full expression $\Delta I(s)$ may be simplified as $I(s)$ or I.

The dynamic equation of the power source is:

$$u = U_{ol} - R_s i - M_s \frac{di}{dt}$$

Its frequency domain expression (Fourier Transform) is:

$$\Delta U(s) = -R_s(T_p s + 1)\Delta I(s) \tag{2.11}$$

Where M_s is the power source inductance, $T_p = M_s/R_s$. Must be noted is that the dynamic response of modern electronic power supplies which use electronic inductance may not comply this derivation. But it is quite reasonable to apply such kind of "first-order inertia system" model to most power supplies in the interested frequency range.

The power outputted voltage is distributed to the arc and stickout wire:

$$u = u_a + u_s$$

Or: $$\Delta U(s) = \Delta U_a(s) + \Delta U_s(s) \tag{2.12}$$

As to arc voltage-current characteristic, the arc can be considered as a no-inertia load, because it has much higher frequency response than our interested frequency range (arc scanning less than 40 Hz). Thus the dynamic model is:

$$\Delta U_a(s) = K_a \Delta L_a(s) + R_a \Delta I(s) \tag{2.13}$$

The stickout is pure resistance load (no inertia) but Equation 2.4 is nonlinear. The dynamic equation can be obtained by linearization with 2-dimensional Taylor's expansion at a set point (I_0, L_{s0}), then taking Fourier Transform:

$$\Delta U_s(s) = K_l \Delta I(s) + K_I \Delta L_s(s) \tag{2.14}$$

Where $K_l = K_s L_{s0}$, $K_I = K_s I_0$.

The wire-melting characteristic is also nonlinear, and has inertia. Firstly, Equ.2.5 can be linearized:

$$\Delta V_m = K_c \Delta I + K_r \Delta L_s \tag{2.15a}$$

Where $K_c = K_m + 2K_e L_{s0}$, $K_r = K_e I_0$.

According Halmoy, the dynamic equation of melting is:

$$j^2 - \frac{J_0^2}{V_{m0}} v_m + \frac{\phi}{\rho_l} \frac{d}{dt}\left(\frac{j}{v_m}\right) = 0 \tag{2.15b}$$

Where j is current density in the feed wire, ρ_l is the resistivity of the hot end of stickout wire, ϕ is a constant, (J_0, V_{m0}) is the set point (static balanced point). By taking linearization and Fourier Transform, we get:

$$\frac{\Delta V_m(s)}{\Delta J(s)} = \frac{2V_{m0}}{J_0} \frac{(T_m/2)s+1}{T_m s+1} \tag{2.15c}$$

Where $T_m = \phi/(\rho_l V_{m0} J_0)$.

However this model is contrary to Halmoy's static model: According to this equation, it turns out that the arc heat has no contribution to wire melting, or said in another way that the stickout Joule heat is the only source energy of melting. With a bit more detailed analysis, it can be found that the static solution of Equation 2.15b is: $v_m/V_{m0} = j^2/J_0^2$. That means the melting rate is proportional to current squared.

But the authors would make use of the time constants from this model, combine them with Equation 2.15a to form another dynamic model of wire melting:

$$\Delta V_m(s) = (K_c \Delta I(s) + K_r \Delta L_s(s)) \frac{(T_m/2)s+1}{T_m s+1} \tag{2.15d}$$

In dynamic state (or the transient period), the melting rate no longer balances the feed rate, the difference results in the arc and stickout length changes:

$$l_s = \int (v_f - v_m) dt$$

Or: $$\Delta L_s(s) = \frac{1}{s}(\Delta V_f(s) - \Delta V_m(s)) \tag{2.16}$$

At a stable welding condition, the wire feed rate is fixed, therefore $\Delta V_f(s) = 0$,

$$\Delta L_s(s) = -\frac{1}{s}\Delta V_m(s) \tag{2.16a}$$

Equation 2.7 is always valid. Its dynamic expression is:

$$\Delta H(s) = \Delta L_a(s) + \Delta L_s(s) \tag{2.17}$$

Now the arc sensor dynamic model, which describes the relationship between CTWD change and arc current change, can be derived by solving Equations 2.11 to 2.14, 2.15d and 2.16a, 2.17. In the following expression, the symbol Δ is suppressed for simplicity.

From Equ. 2.16c and 2.15b, we get Equation 2.18:

$$\begin{aligned} L_s &= -\frac{1}{s}(K_c I + K_r L_s)\frac{T_m/2\cdot s+1}{T_m s+1} \\ &= -\frac{K_c(T_m/2\cdot s+1)}{T_m s^2 + (K_r T_m/2\cdot s+1)}\cdot I \end{aligned} \tag{2.18}$$

Substitute it to the other equations, the following dynamic model of arc sensor is obtained:

$$\frac{I(s)}{H(s)} = -\frac{K_a(T_m s^2 + (1+K_r T_m/2)s + K_r)}{b_3 s^3 + b_2 s^2 + b_1 s + b_0} \tag{2.19}$$

$$b_3 = R_s T_p T_m$$

$$b_2 = R_s T_p(1+K_r T_m/2) + (R_s + R_a + K_l)T_m$$

$$b_1 = R_s T_p K_r + (K_a - K_l)K_c T_m/2 + (R_s + R_a + K_l)(1+K_r T_m/2)$$

$$b_0 = (K_a - K_l)K_c + (R_s + R_a + K_l)K_r$$

The static gain (when s=0) is:

$$\frac{\Delta I}{\Delta H} = -\frac{K_a}{(R_s + R_a + K_l) + (K_a - K_l)K_c/K_r} \tag{2.20}$$

This value (absolute value) should be the same as the sensitivity of static arc sensor, S_{st}.

Equation 2.19 shows that the relationship between the arc current changes and CTWD changes is a third-order model when the power source and wire melting are first-order systems.

When the power source has a very quick frequency response, we can assume T_p=0, that is, no inertia exists. This could be true for invert type power supplies that are the most commonly used now. Then Equation 2.19 becomes second-order system. When the inertia of the wire melting rate to arc current change can also be neglected (T_m =0), the system becomes a first-order system.

However it is difficult to discuss the characters of the system without quantifying it. The next subsection discusses the amplitude and phase response of the system, which is critical to high speed spinning arc sensor properties.

2.3.2 Discussion on Arc Sensor Dynamic Models

By substituting the parameters in the dynamic model, the system poles, zeros and frequency response can be calculated. During the research the MatLab software was used to do these calculations.

With references, a set of parameters, which may not be exactly fit for any real condition, but are within the reasonable range of GMAW, is chose as follows:

Wire cross-section area: A=1.13 mm^2, (solid wire diameter 1.2mm),

Power supply output drop slope (source resistance): R_s=2V/100A=0.02Ohm,

Arc column electric field intensity: K_a=1.0 V/mm, (range: 0.5~2)

Arc slope resistance: R_a=0.04Ω, (from reference arc load: U=20+0.04I),

Average stickout wire resistivity: ρ=1.0 mΩ·mm, then voltage drop constant: K_s=0.0009 V/(mm·A).

Arc heat melting constant: K_m=0.3(mm/s)/A, (Lesnewich: 8~10lb/hr/500A),

Resistance heat melting constant: K_e= 0.000067(mm/s)/(mm·A^2),

Set point current: I_0=200A, then current density is: J_0=176A/mm^2.

Set point wire feed then is: V_{m0} = 100 mm/s.

Set point stickout length: L_{s0} =15mm,

Set point arc length: L_{a0} = 6mm.

The melting model time constant: T_m =0.165 second, this is calculated from Equation 2.15c: $T_m=\phi/(\rho_l V_{m0} J_0)$, where the resistivity of hot end of wire ρ_l = 1.2 mΩ·mm and ϕ=3.5 V are typical values for mild steel.

Set the power source time constant T_p = 0.003s, this is corresponding to a cut-off frequency (-3dB) at 53 Hz.

With this set of parameters the model is evaluated as:

$$\frac{I(s)}{H(s)} = -3.46 \frac{0.01685s^2 + 0.4575s + 1}{1.28\times10^{-5}s^3 + 0.01576s^2 + 0.1776s + 1}$$

The static value (substitute with s=0) is 3.46 A/mm, which means the static arc sensor sensitivity. The zero points of the system are: $z_{1,2}$ = -3.78 ± 1.58j. The poles are: $p_{1,2}$ = -5.7±5.7j, p_3 = -1217.

The amplitude and phase response to frequency of $-\Delta I/\Delta H$ is shown in Figure 2.3. Three special points in the curve must be noticed. These points are corresponding to the zeros and poles of the system.

$\omega_1 = \mid z_{1,2} \mid = \sqrt{3.7^2 + 1.58^2} = 4.02$ radians/second, or $f_1 = 0.64$Hz.

$\omega_2 = \mid p_{1,2} \mid = \sqrt{5.7^2 + 5.7^2} = 8.1$ rad/sec, or $f_1 = 1.28$Hz.

$\omega_3 = \mid p_3 \mid = 1217$ rad/sec, or $f_3 = 194$Hz.

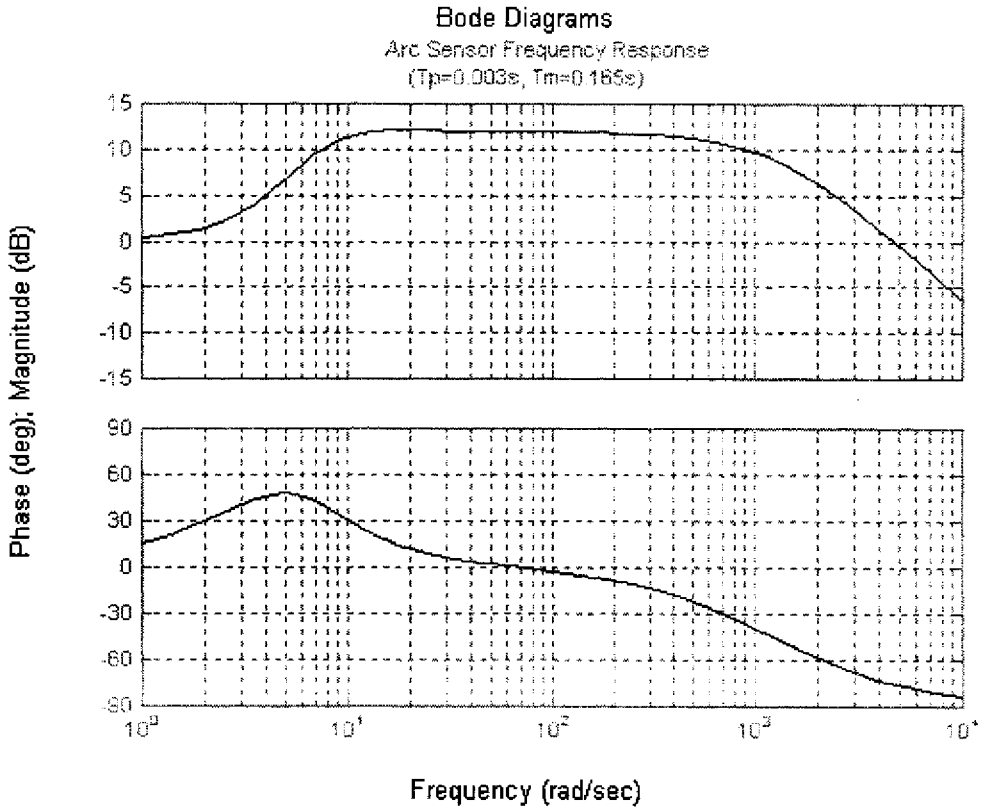

Figure. 2.3 Simulated frequency response of arc sensor

In Figure 2.3, it is shown that between the frequency of 30rad/sec (~5Hz) to 300rad/sec (50Hz), the amplitude response has a flat and high value. This range is within ω_2 and ω_3. It means that when CTWD changes as a sinusoidal function at this frequency range, each unit of CTWD change causes higher arc current change, that is, the arc sensor has higher sensitivity. This figure shows the increase compare to static state is 12dB, or 4 times. That is the static sensitivity I/H is -3.64A/mm, the dynamic sensitivity $\Delta I/\Delta H$ is -14.5A/mm.

The figure also shows the phase shift of the output (current) to the input (CTWD). When processing arc sensor signals, this must be take consideration because such a shift will affect the corresponding of signal to actual arc spinning position.

2.4 Relationship between Arc Current Waveform and Torch-Joint Deviation

When the arc is spinning over the groove as shown in Figure 2.4, the theoretical current waveform is as shown in Figure 2.5. In this simulation, the melting delay is neglected (T_m=0) and thus the arc sensor model has form of:

$$I(s)/H(s)=K_0(T_1 s+1)/(T_2 s+1)(T_3 s+1) \tag{2.21}$$

The spinning speed is 20Hz; spinning diameter 6mm, torch is 2mm to the right of the joint center. The inference of weld deposit on the distance from contact tip to weld surface is not considered.

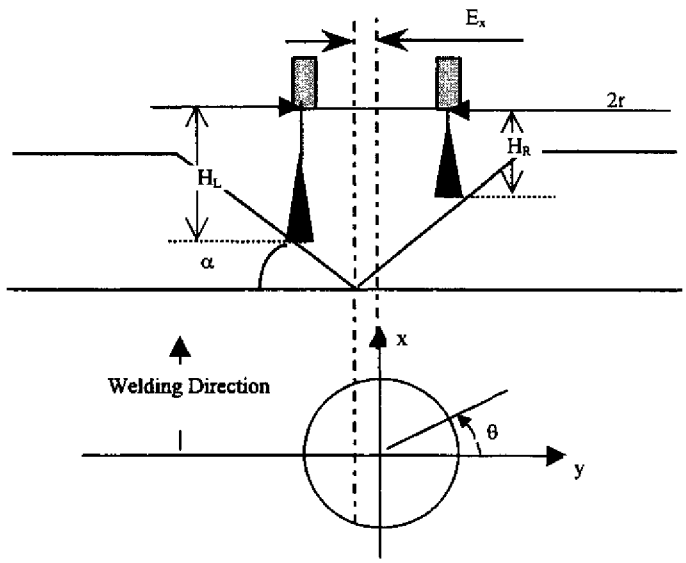

Figure 2.4 Illustration of arc-joint geometric relation.

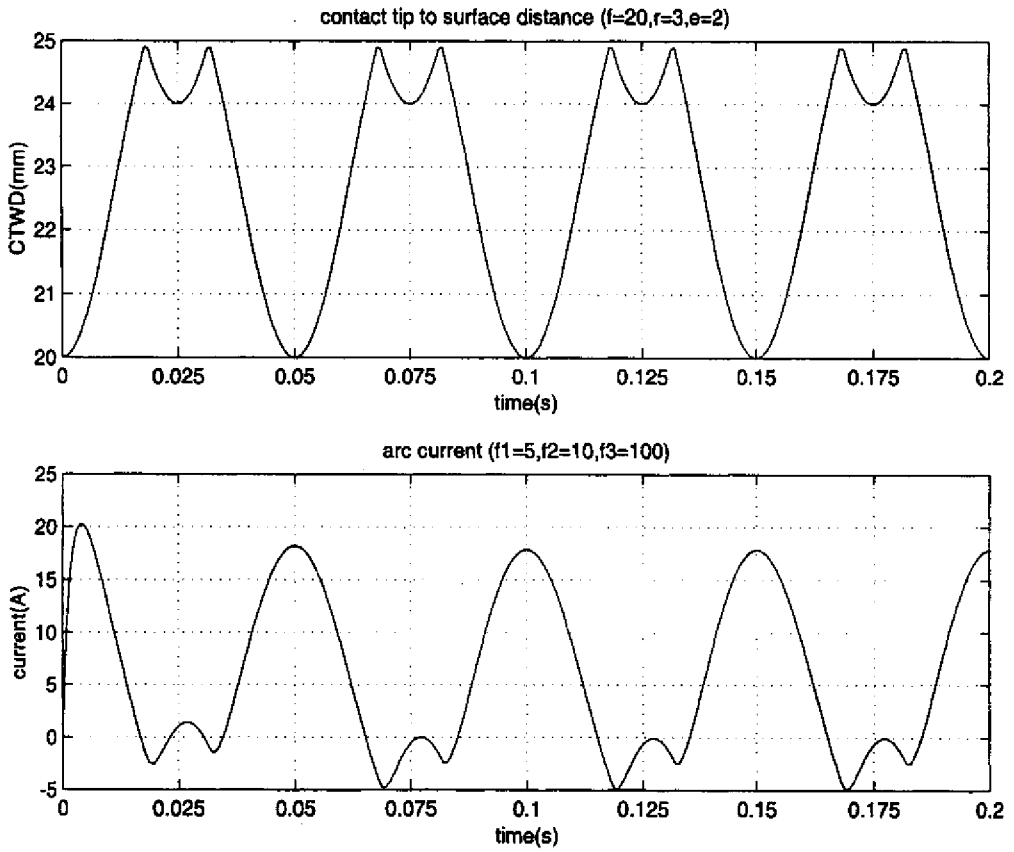

Figure 2.5 Arc sensor signal waveform simulation, spinning at 20 Hz, deviation Ey=2mm, groove angle α=45°.

In this example, as the torch spinning center is at right of the joint center, the current at the right side is higher than that of the left side. The difference of the sum of current at the left half of the spinning circle subtracted from the sum of current at the right half of the spinning circle indicates the torch-joint deviation. This value is considered the output of the arc sensor. The formula can be described as:

$$E_y = \frac{1}{S_{dy}}\left(\int_{-\pi/2}^{\pi/2} i(\theta)d\theta - \int_{\pi/2}^{3\pi/2} i(\theta)d\theta\right) \tag{2.22}$$

Where S_{dy} is the dynamic sensitivity ($\Delta I/\Delta H$), that is, the amplitude of Euation 2.19 at the spinning frequency.

When the result is positive, the torch deviates to the right of the joint. Mathematical analysis shows that with the deviation less than 0.7 of the spinning radius, the relationship is perfect proportional; in the range of 0.7 to 1.0, it is still close to proportional but when the deviation is more than the spinning radius, the computed value (arc sensor output) is the same as that when the deviation equals to the radius.

However in practical welding, the current waveform is far from the simulation as shown in Figure 2.5. A more sophisticated signal processing algorithm is required, which is discussed in next chapter.

CHAPTER 3

SETUP AND TESTS OF THE PROTOTYPE SYSTEM

3.1 Underwater FCAW System Setup

The underwater FCAW system includes a welding power source, a wire feeder, welding torch, the welding head carrier for mechanized welding and a shielding gas supply. Most of the tests were performed in a small experimental tank with a mechanized side beam carriage for easy of operation. Some testing has been done in an 8-feet-deep dive tank in the weld laboratory at The Ohio State University. The wire feeder is placed on the surface for tests in both tanks.

The small tank dimensions were 30" deep, 48" long, and 36" wide. There is a transparent view window on the front wall of the tank. Welding could be performed underwater up to 20" depth and travel for 24".

From the results of previous research and early tests in current project, self-shielding stainless welding wire SOS 308L was used as the filler material in this study. Commonly used low carbon steel (mostly A36) was used for the base metal.

An ovoid contoured shroud with sponge skirt is used to provide shielding of the arc and weld pool from the intruding water, and to retard the weld and heat affected zone cooling. Our study in the earlier projects (Sea Grant Program sponsored) had concluded this could improve the weld quality significantly.

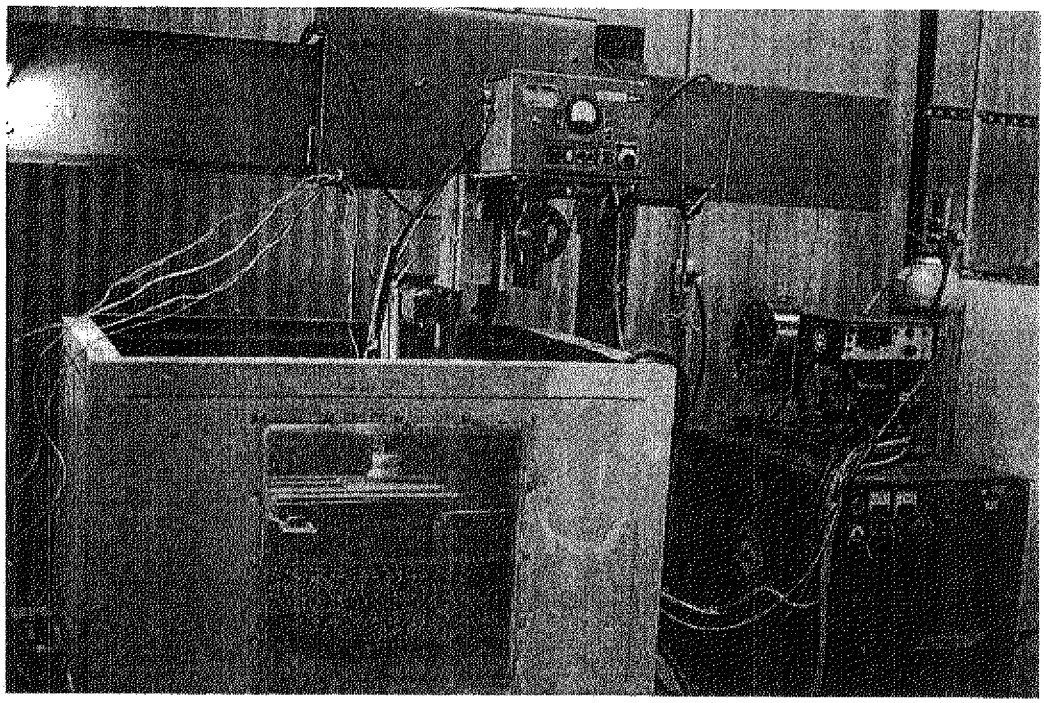

Figure 3.1 Picture of the mechanized underwater welding system.

3.2 Development of High Speed Spinning Torch

According to study reported in the previous chapter, in order to reach high arc sensor sensitivity, the frequency of the arc scanning across the joint grove must be in a higher range. Another no less important point is that at a higher scanning frequency, more information is acquired in a given time. Thus the system response can be quicker than for low frequency scanning.

3.2.1 Spinning Mechanism

The back and forth movement of the arc across the joint groove can be realized mechanically or magnetically. While the magnetic field can control the arc moving range and frequency, the actual arc position is not easy to control and measure with this method. Arc scanning induced by the mechanical movement of the contact tip can be controlled much more precisely.

Usually a circular movement make it easier to reach high frequencies and has simpler mechanical assembly than a periodic back and forth linear movement. Therefore a circular

scanning arc sensor mechanism was adapted in this study. But for welding torch, as the contact-tip is rigidly connected to the conduct rod, and the conduct rod is attached to the welding cable, the feed wire goes through the core of them, a special design is required to make circular movement possible and avoid wire twisting.

An innovative hollow-shaft motor directly driven mechanism was developed. In this mechanism, a pair of self-aligning bearings connect the conduct rod to the hollow shaft of the motor. The conduct rod is eccentric to the nominal centerline at one end. This structure makes the rod move in a circular swing (cone-pendulum) and the arc spins over the joint at the motor rotation frequency. The contact tip does not self-rotate, so the feeding wire does not twist and the welding current can be introduced to the torch directly with a piece of flexible cable. With no additional transmission mechanism, the minimum size was reached.

The motor is specially designed for this application. As normal housed small profile motors can not provide a large diameter shaft, the researchers have designed the housing and shaft for a rotor and stator set. The motor itself has a dimension of ϕ46mm×32mm (ϕ1.8"×1.3"). Including the encoder and eccentric structure, the length is about 85mm (3.4"). The torch can be mounted onto a carriage for mechanized welding or held by a welder with the handle. Figure 3.2 shows the picture of the assembly of the high-speed spinning torch.

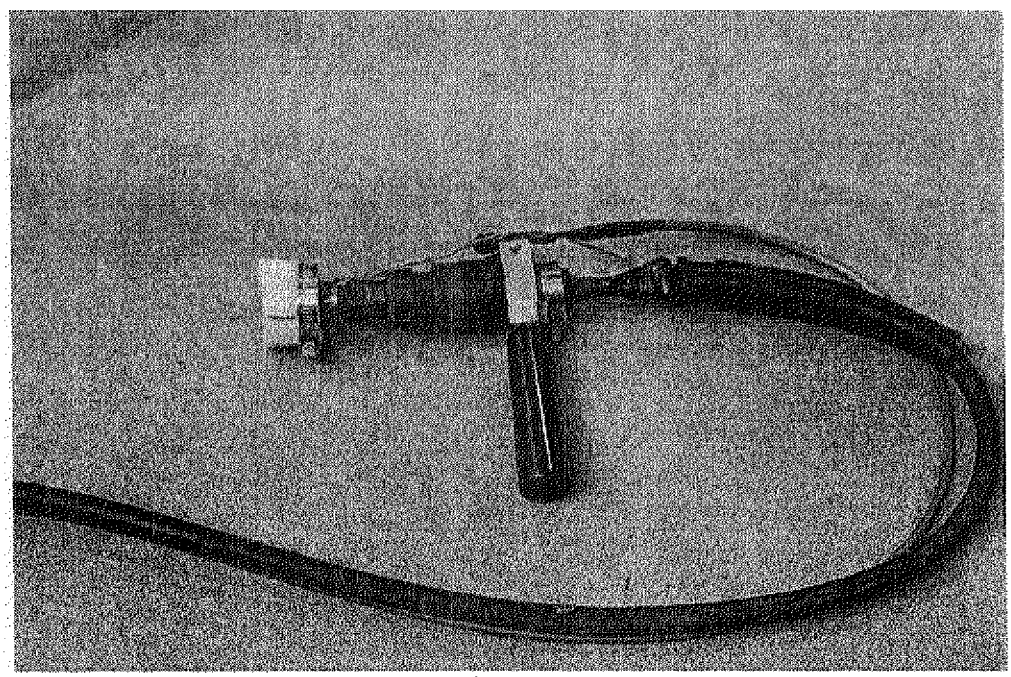

Figure 3.2 Picture of spinning torch

3.2.2 Spinning Arc Position and Speed Detection

A two-phase incremental optical-electric encoder was installed inside the motor to detect the arc scanning position and the rotation speed. One revolution is divided to 64 positions, with one marking at the start of the revolution. The frequency of the output pulse of the encoder indicates the rotation speed of the motor. A frequency-to-voltage circuit is used to make this conversion. A motor driving module uses this signal to compare to the required set speed to realize feed back control of the motor speed. This control ensures smooth and stable movement over a wide speed range.

The arc position is determined by the indexing pulse numbers elapsed since the marking pulse. The arc parameters (mainly arc current) are analyzed against the arc position to find the relationship between them and the joint groove geometry.

The arc spins in a counterclockwise direction in the top view. The right end (3 o'clock position) of spinning (when welding forward) is defined as start point of a scan.

3.2.3 Waterproofing of the Torch

The motor and encoder are required to be sealed. With this innovative mechanism, the conductor rod and tip not self-rotating, so flexible sealing nipples can be placed between the two ends of motor housing and the conductor rod. For simplicity, in the testing prototype, silicone sealant was applied directly at these two positions to make the motor waterproof. Tests show that the sealant can provide satisfactory waterproofing while allowing the conduct rod to swing.

3.2.4 Spinning Torch Features

Spinning frequency: 4~33Hz adjustable;

Scanning diameter: 3.5mm fixed;

Positioning resolution: 64/rev.;

Dimension (approx.): ϕ46mm×180mm (ϕ1.8"×7.1").

Driving circuit: DC 24V, 4A;

Control circuit voltage: DC 5V.

3.3 PC Based Control Unit and Interface

A desktop PC system was applied at first as the control unit as there is commercially available data acquisition hardware and processing software for the PC platform. The better human-machine interface for the PC based system also makes the research work more convenient.

This system consists of a host computer, a data acquisition board with A/D converters and digital I/O ports, signal conditioners, spinning position sensor signal preprocessing board and an isolated arc current sensor (Hall effective device). A common PC will fulfil the requirements of this system.

3.3.1 Computer Interface

The requirement for the A/D converter includes mainly the resolution and sample rate. As the resolution of arc spinning position is 64/rev and the maximum spinning speed may up to 50Hz, the maximum data rate is 3.2KHz. As arc current rages from 0 up to 500A, at least a 10-bit A/D converter, which gives a resolution of each digit interval equaling to 0.4 ampere (this equals to 0.2mm CTWD change, referred to section 2.2.2), is required. A DAS-1602 interface board featuring 16-channel, 12-bit A/D conversion, two-channel, 12-bit D/A conversion, and three 8-bit digital I/O was used in the system.

The input port was set as single end, with reference voltage of 10V, that is, input range is 0~10V, and is digitized to 0~4095. Signals such as arc current, voltage, and the gas cavity temperature in the shroud, are connected to the analog inputs. The analog output port is used to send the driving signal of the actuator for automated feedback control. Arc spinning position codes were connected to digital and interrupt port for triggering A/D converter.

Figure 3.3 shows the block diagram of the system. Figure 3.4 is the photograph of the PC and the interface circuits.

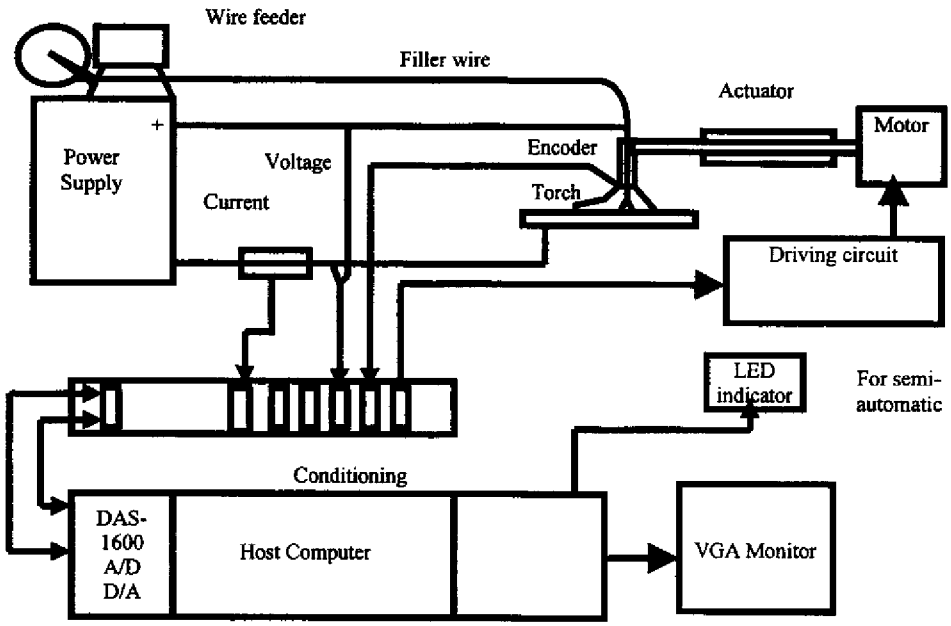

Figure 3.3 Block diagram of the PC based system

All analog signals are connected to the A/D board through isolation/conditioning modules. Digital signals are connected to the board through optocouples. The isolation reduces the risk of the arc current or voltage surges interfering the computer electronics.

Arc voltage is detected at power supply terminals. With ladder resistance, a partial of the voltage (with reduction ratio of 75V: 3.6V) is input to the conditioning module 5B31 (from Analog Device) with a ±10V: 5V transfer ratio.

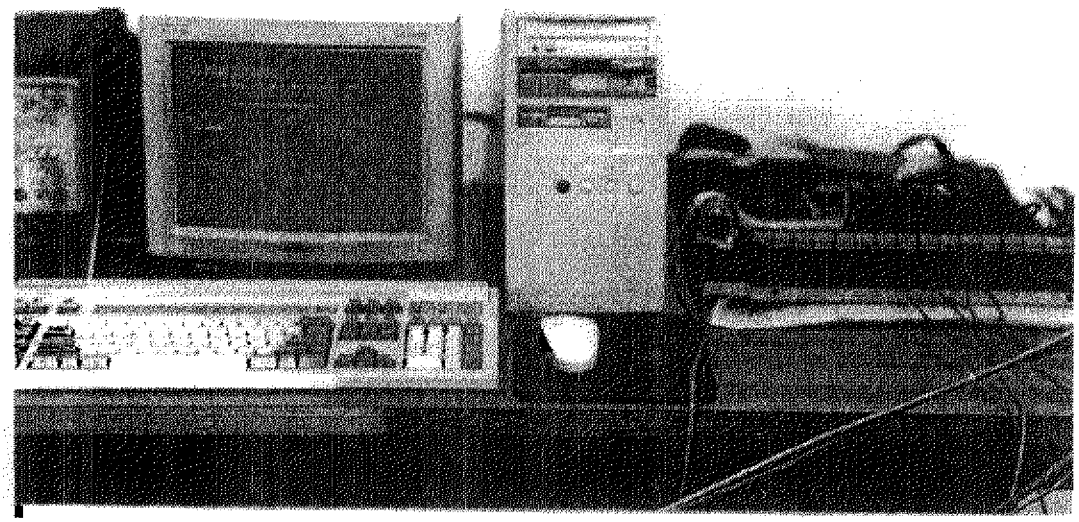

Figure 3.4 Picture of the PC based control system

Arc current is measured with a Hall effect device, which has no electrical connection to the welding power circuit. The transmission ratio is 500A:100mA. With a 50-Ohm resistance it is converted to voltage signal. Through a ±5V: (0~5V) signal conditioning module 5B41, the current signal is connected to A/D channel 10. A current of 0~500A is converted to digit 2048~4095 (with an internal gain of 2 of the A/D board).

The D/A channel for controlling the actuator is set to bipolar with reference voltage of 10V. That is the output voltage is within ±10V.

3.3.2 Seam Tracking Actuator for Mechanized Welding

Most of the study was done with mechanized welding for saving labor and reduction of human factors. A DC motor driven electrical cylinder is mounted on the welding carriage to adjust the transverse position of the torch to the center of the joint. A DC motor driving module is used to control the movement of the cylinder. A tachometer is mounted on the motor to measure the spin speed. The driving module compares the set value and the actual spin speed to adjust the voltage supplied to the motor to reach the required speed. The set value is from the PC through

the D/A channel. A pendant provides manual control of the driving module to adjust the torch position.

Figure 3.5 shows the picture of the torch installed on the actuator.

Actuator features:

Stroke: 200mm (8");

Voltage: 24V;

Maximum speed: 21mm/s

Control ratio (tachometer gain): 1.76 (mm/s)/V.

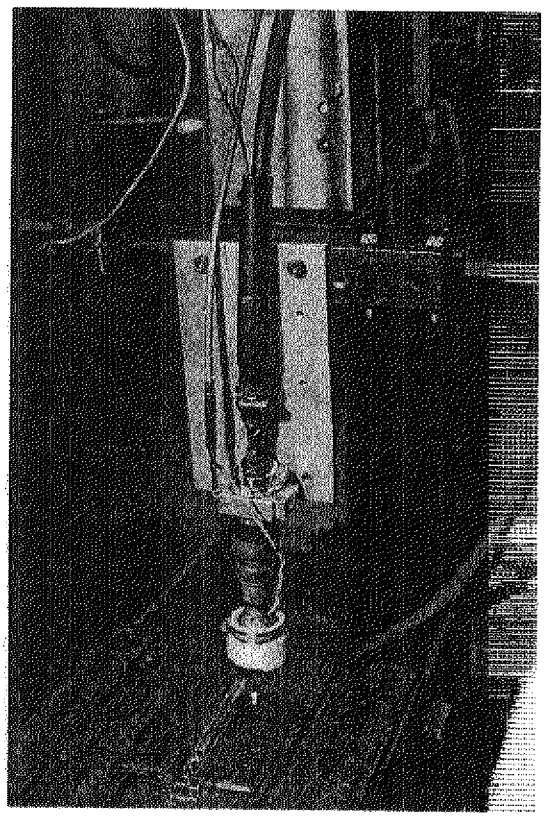

Figure 3.5 Picture of Spinning torch installed on a motorized slide

3.4 Control Algorithm and Programming

3.4.1 Data Acquisition

As arc sensor signals need be analyzed against the arc position, the arc parameters and arc position must be sampled accordingly. A simple and effective method is using the position signal (electric pulse) from the optical encoder to trig A/D conversion and save the data to the computer memory in a designated structure. The arc position information can then be retrieved from the data structure.

The DAS-1602 A/D board has an external trigger, external pace clock operation mode. When set, a pulse at the "external trigger" pin enables the A/D converter to sample and convert analog signal at the frequency of the external pulse on the "pace clock" pin. This mode was used in the study.

3.4.2 Signal Filtering

The arc current signal was found to be fluctuating seriously due to the disturbance of short circuit, spatter, melting drop transfer and arc polar spots moving. Basically use of low pass filters is applicable for this system. A simple R-C analog filter with a higher cut-off frequency is used to attenuate high frequency noise. It does not affect the signal at the frequency of arc spinning. Digital (software) filters played a main role in reducing low frequency noise, as digital filtering is more flexible, easier to adapt and can be designed to inducing no phase shift (between resulting signal and the actual spinning arc angular position) at the spinning frequency.

Several digital filtering methods were studied. Combining the multi-cycle average method and the symmetric sliding window average shows effective and satisfactory results. Multi-cycle average is the method that calculates the signal value at an arc spinning position by averaging the data of the same position at several different scans.

The formula for this filter is:

$$i_{f1}(n) = \frac{1}{N_{ma}} \sum_{k=0}^{Nma-1} i(n-64k) \; ; n = 1,2,\ldots 64 \qquad (3.1)$$

i is sampled original current signal; i_{fl} is filtered arc current; n is the arc position index; N_{ma} is the numbers of scans taken to average.

Symmetric sliding window average is a filter that calculates the value at a position by the average value of several positions before and after this position.

The formula for the filter is:

$$i_{f2}(n) = \frac{1}{2N_{sl}+1}\sum_{k=-Nsl}^{Nsl} i_{f1}(n+k) \; ; n = 1,2,\ldots 64 \tag{3.2}$$

i_{f1} is the resulted signal of the first filter; i_{f2} is filtered arc current; n is the arc position index. N_{sl} is the half-width of the window. A sliding window length of 9~15 is proved proper for FCAW by experiments.

Neither filter introduces phase shift with respect to the arc spinning position. But they introduce time delay, which means the results obtained are actually what the values were a short time ago. This delay can be reimbursed with feedback control logic.

3.4.3 Torch to Joint Center Deviation Computing

This computation is based on the discrete type of Equation 2.22. But the phase shift of arc current to CTWD and weld deposit is taken into consideration. The authors used a more sophisticated approach, based on spectrum and correlation analysis to get more reliable results. The details of the method can be found in the control code (listed in Appendices). Here a simple explanation of the process wil be given.

Using test-learning welding, the phase shift at a set frequency can be determined. In this test, the torch lays a bead-on-plate weld at a push angle of about 30°. The deposit and the push angle have the same effect on CTWD change: longest at the front and shortest at the rear point. When the right end of spinning circle (refer to Figure 2.4, θ=0) is defined as the start point, index k=0, the front point is indexed k=16, rear end k=48. The deviation to the peak point of current waveform to the rear point is the phase shift. This can be corrected in programming.

As the deposit caused CTWD change is 90° out of phase with the weld groove caused CTWD change in ideal conditions (as bead-on-plate), When the system model is linear, its effect will be eliminated by equation 2.22. In a grooved welding, the deposit caused CTWD change and the groove caused CTWD change (when transversal deviation exists) may be coupled.

A weighted average, instead of the simple sum and subtraction is used to calculate the arc sensor output. It is a simple implementation of correlation analysis that provides further filtering effect. The mathematical expression is:

$$E_y = \sum_{k=0}^{63} i_{f2}(k)\cos(2k\pi/64) \tag{3.1}$$

3.4.4 Feedback Control Logic

Once the deviation of torch to joint center is found using the above method, the electrical cylinder can correct the torch position in mechanized welding. The information can also be uesd to visually guide the diver/welder to adjust the torch position in both mechanized or hand held welding.

In automatic feedback control, PID (proportional-integral-differential) adjust mechanism is a traditional yet effective method in this application. The mathematical expression is:

$$v_g(n) = K_P E_y(n) + K_I \sum_{k=0}^{n} E_y(k) + K_D(E_y(n) - E_y(n-1))$$

v_g is the voltage sent to the actuator driving circuit, representing the required actuator speed. In practice it is modified so that this voltage is decided by the current and of several previous deviations:

$$v_g(n) = \alpha v_g(n-1) + \sum_{k=0}^{N} \beta(k) E_y(n-k) \tag{3.2}$$

Figure 3.6 shows the logic diagram of the feedback control of seam tracking.

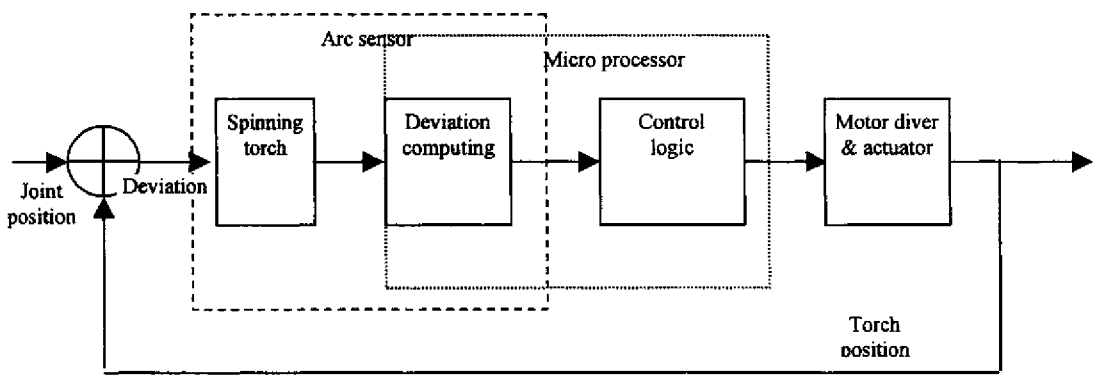

Figure 3.6 Control logic block diagram of weld joint tracking with arc sensor

3.4.5 Programming

This control program was written in C language. The code is listed in appendix. Figure 3.7 is the flowchart the program.

In a real-time control system, an important point is the controller must be able to respond to the real world in time. Although the sample rate of the arc sensor signal is not high (1.28KHz at 20Hz spinning frequency), the program must processing signal filtering, deviation calculation, and PID adjust computation simultaneously. Background data acquisition is used in the program. When the CPU is processing (filtering, correlation calculation and PID adjustment) the previously acquired data, the A/D board is background sampling arc the current without the control of CPU. The arc current waveform is also graphically displayed against the arc spinning position on the computer screen. This graph gives virtual groove geometry. Arc current and other data can be saved as disk files for later analysis. A software watchdog was programmed to resume the program from dead-loop in A/D conversion caused by triggering or clocking pulse error.

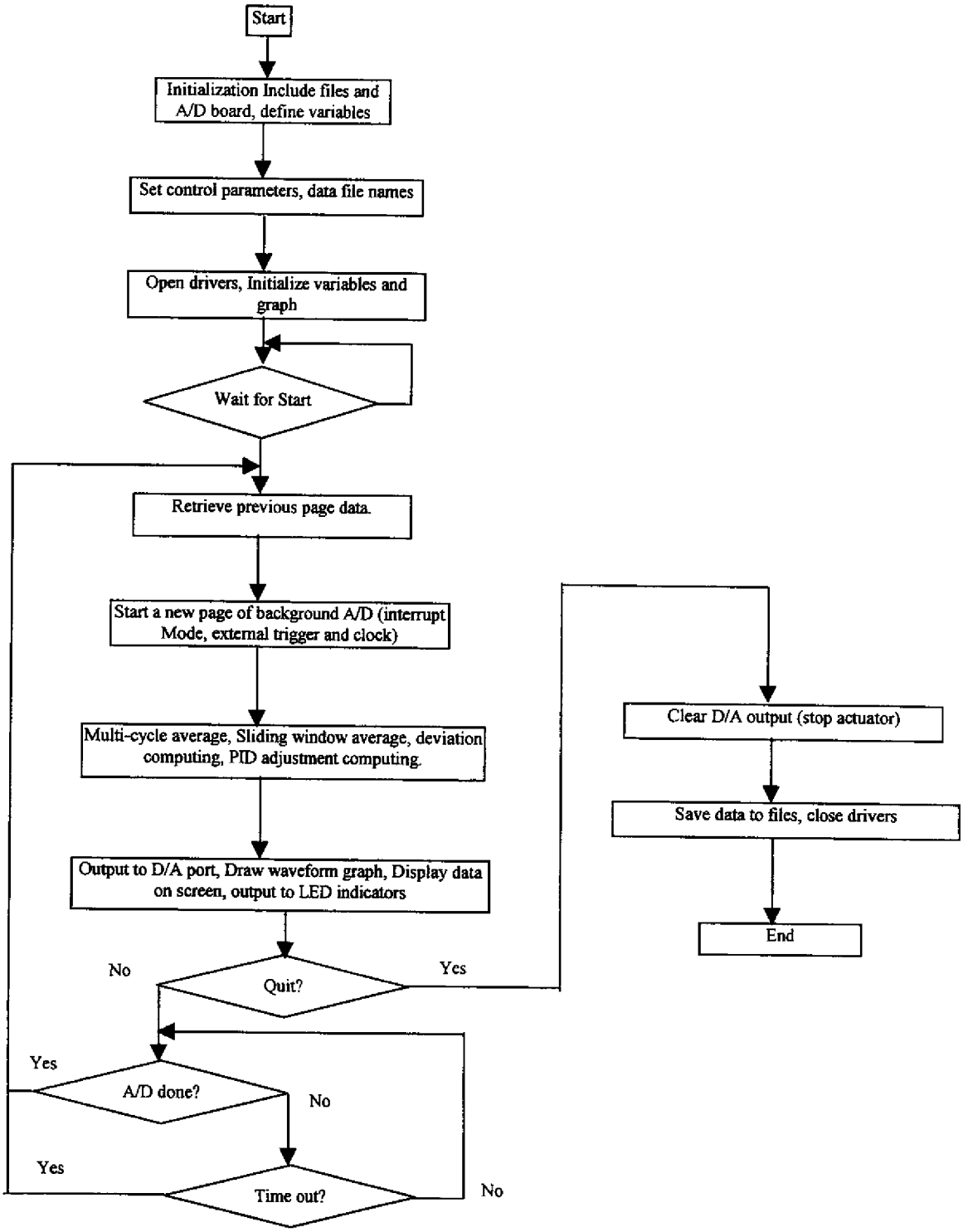

Figure 3.7 Arc sensor signal processing and feedback control flowchart

3.5 Tests and Results of Arc Sensor Signal Processing

3.5.1 Welding Arc Current Waveform Processing

Figure 3.8(a) shows a waveform of the welding current when the arc spinning over a right side raised flat plate. As the short circuit current may be over 500A, and the current change caused by arc spinning and joint groove is only about 5~30A, the signal to noise ration (S/N) is poor. As a matter of fact, it is hard to see any information about the torch to welding joint center deviation from the raw current waveform. Figure 3.8(b) is the filtered waveform. It shows obviously the current changes when the arc spinning causes the contact tip to workpiece surface change.

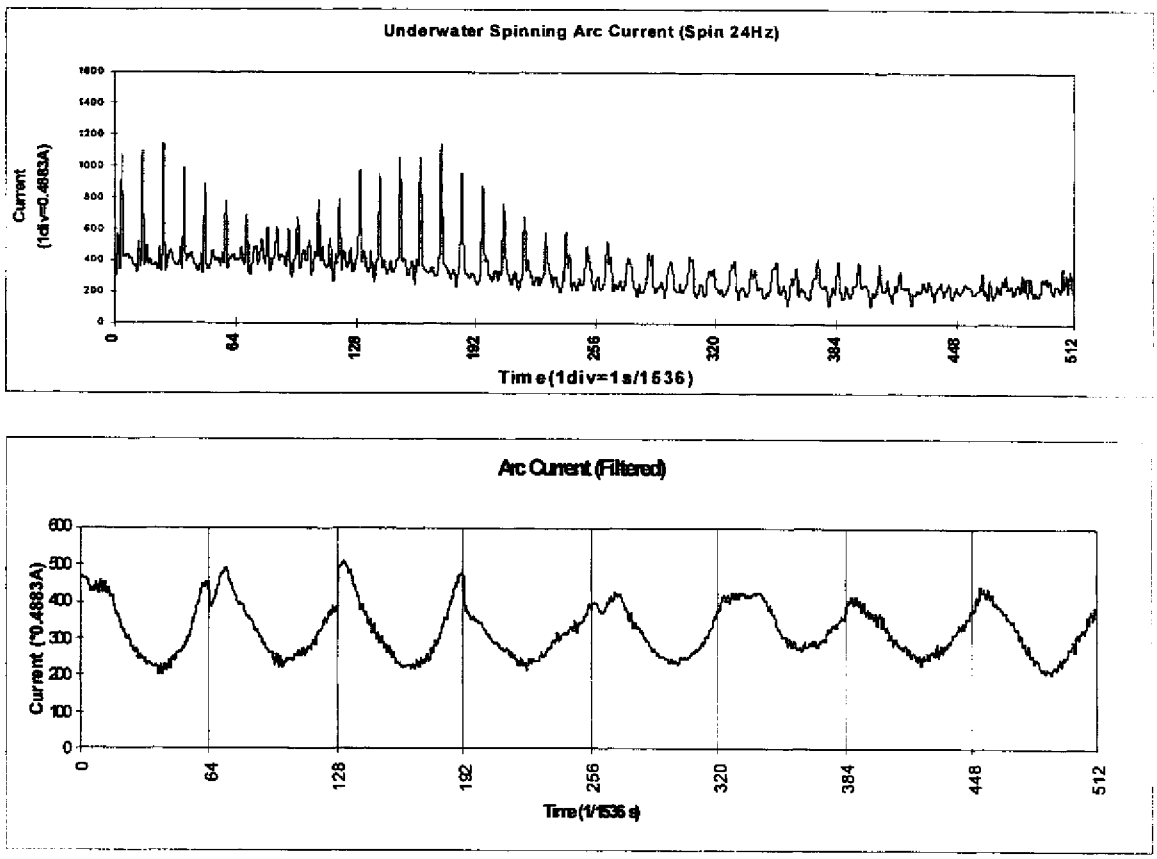

Figure 3.8 Arc current waveform (a) original samples, (b) filtered result

3.5.3 Experimental Results of Dynamic Arc Sensor

The theoretical analysis in section 2.3 was verified by experiments. Bead-on-plate welds were deposited with the torch at a push angle of 20°. This set up eliminated the weld deposit inference on phase shift. The first group was tested in air with 308L stainless steel and no shielding gas. The weld bead appearances are almost same, therefore the actual contact-tip to weld surface distance change patterns are the same for different frequencies. In order to get more accurate and reliable results, a number of scan circles of signal were averaged using method mentioned in section 3.2.2. The averaging ranges from 32 to 256 cycles depend on spinning frequency. Figure 3.9 shows the average current waveform against the spinning position. It can be seen that at high frequencies, the arc current waveforms are closer to the theoretical shape, that is, sinusoidal waves. But at low frequencies this characteristic is much weaker. This implies that at high frequency the arc sensor is more reliable.

Table 3.1 and Figure 3.10 show the current changes (peak-to-peak value) when arc spinning at different frequencies. In the frequency range of 13~25Hz, the arc sensor has a higher sensitivity. The curve shape is very similar to the theoretical results reached in section 2.3.2.

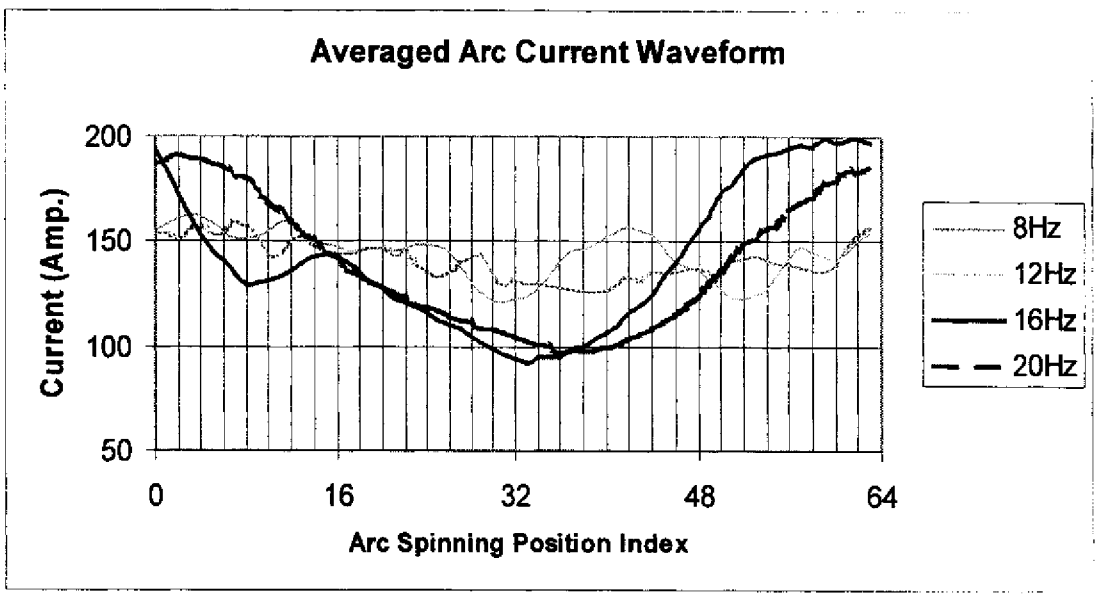

Figure 3.9 Averaged arc current waveform at different spinning frequencies

Table 3.1 Arc current wave peak-to-peak value at different spinning frequencies

Spin Speed (Hz)	Avg.Current (Amp)	P-P Current (Amp)	File Name
2.4	203	13.5	930_025
3.8	200	27.2	930_04
5.8	192	53.9	930_06
7.8	196	43.6	930_08
9.7	195	57.5	930_10
12.7	202	85.8	930_13
15.7	198	73.3	930_16
19.7	196	89.6	930_20
24.6	198	84.0	930_25
29.3	199	57.0	930_30

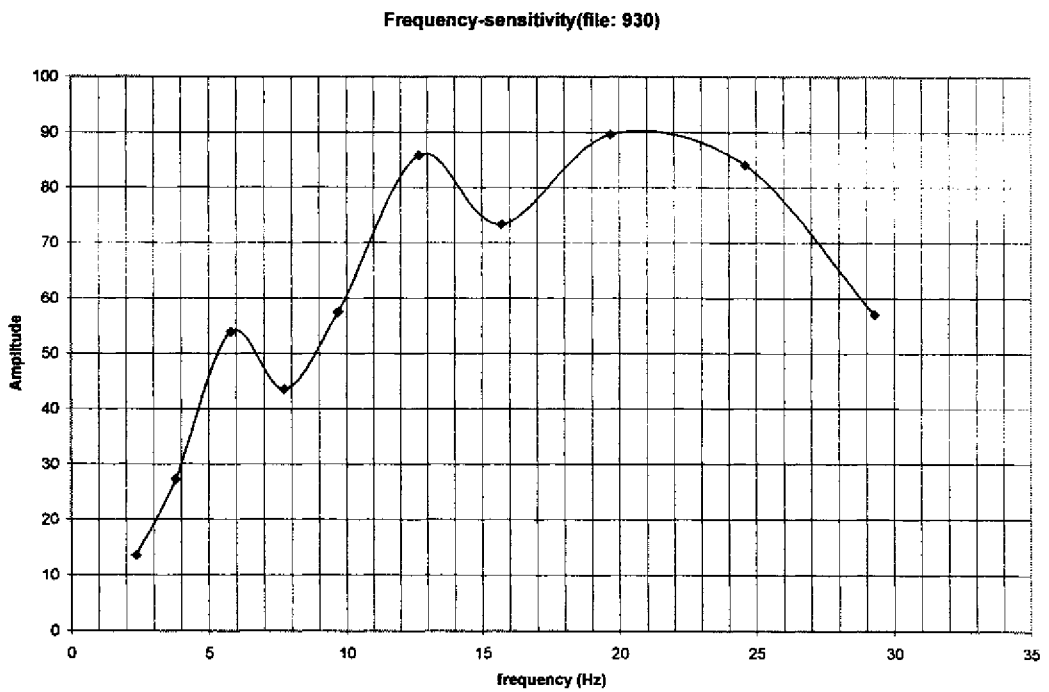

Figure 3.10 Arc sensor sensitivity vs. frequency (in-air welding). CTWD changes about 4mm.

The second group of tests was carried underwater in a water depth of about 8 inches. The welding conditions are the same as the first test group. The results are shown in Figure 3.11. It can be seen that the curve is similar to that of in-air welding results. The high-sensitivity range is 15~35Hz.

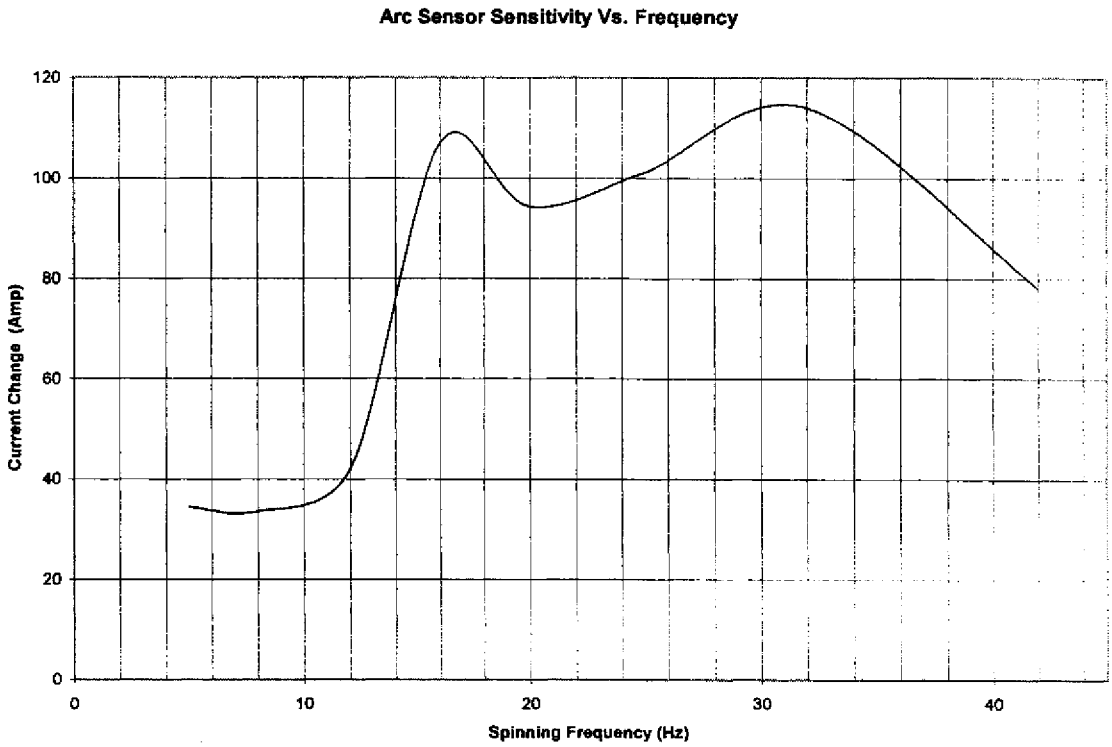

Figure 3.11 Arc sensor sensitivity vs. frequency (underwater welding). CTWD changes 4mm.

CHAPTER 4

DEVELOPMENT OF A COMMERCIAL DEMO SYSTEM

4.1 Control Unit Based on Microcontroller

As mentioned before, the PC based system is convenient for study in laboratory, but it is not suitable for industrial field use. Industrial PCs are well designed for working in such environment. But for this application, a microcontroller (MCU) is more proper because of its small size, low cost and robust and control oriented resources. Microcontroller-based system has the processor embedded in the control circuits, thus it is more like a traditional instrument than a "computer", as usually it has simpler human-machine interface, such as small LCD (liquid crystal display) text screen, indicators, meters, and setting switches/buttons.

A typical microcontroller is a true computer on a chip. The design incorporates all of the features found in a microprocessor CPU. It also has added the other features needed to make a complete computer: ROM, RAM, parallel I/O, serial ports, counters, and a clock circuit. Furthermore, most microcontrollers have some other useful function modules for process control, such as A/D converter, pulse width modulation (PWM), input capture (IC or HSI), comparing output (OC or HSO). Usually a small board with a microcontroller and a fewer port buffers will make a complete functioning controller.

In the design of the commercial prototype, a low cost, small single-board (Freedom v2.5 by Intec Inoventures Inc., size 4.0×6.5×1.0 inches) based on a Motorola M68HC16Z microcontroller is used as the brain of the control unit.

Main features of the single-board microcontroller are:

MCU chip HC16Z1: 16-bit architecture and instructions, dual 16-bit accumulators, digital signal processing capability, address up to dual 1M bytes memory, system clock 16.78KHz, 1K bytes on-chip RAM, three 8-bit digital I/O ports, 8-channel 10-bit A/D converter, 8-channel IC or OC, 2-channel 8-bit PWM, two 16-bit counters, serial communication port.

Board extended: RAM 64Kbyte, EEPROM (Flash Memory) 256Kbyte. RS232 and RS485 communication ports, two 12-bit D/A channels, a keyboard and LCD port.

The hardware resources of this unit are enough to serve as the welding seam tracking controller.

4.2 System Integration

The microcontroller unit must have the same functions as the desktop computer: welding parameter acquisition, processing, arc current waveform pattern recognition and seam tracking feedback control or deviation signal display. But both the hardware and software resources and features are totally different. With the microcontroller, many of the on-chip resources can be made use of. The A/D board and conditioning modules used in the PC system are not needed here.

4.2.1 Microcontroller Resource Allocation

The input and output signals are the same as in the PC based system. The hardware wiring are assigned as:

Arc current signal from Hall effect sensor is connected to A/D channel 0. As Hall sensor isolates the measuring circuit from the welding circuit, the signal can safely be connected to MCU directly (with a peak value limit circuit).

Spinning cycle start marking pulse is connected to Input Capture (IC) channel 1, the indexing pulse is connected to channel 2. The working mode is set to edge sensitive. Each pulse can cause an interrupt request to CPU.

Two PWMs are used as a bipolar D/A to output the setting speed to control the tracking motor. The pulse signal is filtered with an R-C circuit to get the equivalent analog voltage. Channel A gives positive or "move to right" voltage; channel B gives negative or "move to left" voltage.

One 8-bit digital output port (Port 4) is used to drive a linear array LED (light emitting diode) indicators to display the arc-joint deviation and program execution status.

4.2.2 Interfacing Board

In the PC based system, conditioning modules are used. In the microcontroller system, with the well-designed resource allocation, it is possible to use simple and cheap optocouples to

electrically isolate the signals from the MCU. Another small circuit board is used for preprocessing the arc spinning position codes, spinning speed conversion, arc current, and to isolate PWM signals and filtering.

The signals from the encoder inside the spinning torch motor do not match the voltage level of the MCU. They are reshaped through comparing circuits composed of operational amplifiers to improve pulse quality. Then the reshaped pulses are connected to MCU IC pins through optocouples.

The reshaped indexing pulse (64/rev.) is converted to an analog signal through a F/V (frequency to voltage) circuit. This voltage, indicating the arc spinning speed, is used as the feedback signal in the spinning motor driving module.

A potential meter on this board sets the speed of the spinning motor.

As the PWM signals are switch mode, they can be isolated with cheap optocouples. Then a simple R-C circuit is used to filter it to an analog signal. The signal is sent to the tracking motor driver as setting speed. If the signals are filtered first, then a much more expensive and bigger analog isolator is required.

The digital signals sent to the LED indicators can also be isolated with the same method.

4.2.3 System Structure

Figure 4.1 shows the block diagram of the system. Inside the dotted line is the control unit. It consists of the following components:

Microcontroller board;

Interface board;

Spinning motor driving module;

Tracking motor driving chassis;

Power supply for MCU and Hall sensor circuit (inner circuit);

Power supply for external circuit;

Power supply for spinning motor driver.

These components are enclosed in an instrument case as shown in Figure 4.2. The panel is shown in Figure 4.3. The six cables are connected to:

Hall sensor;

Spinning motor;

Tracking motor;

Manual control pendant;

LED indicators;

An auxiliary arc position and current signal output.

The manual control pendant has a switch to set the actuator to be controlled by the controller or manually (switch off automatic tracking), and a momentary 3-postion switch to move torch left or right. One array of LED is installed on the pendant to display the visual signals showing the deviation for manually tracking with the mechanized system. Another array of LED is installed in the diving helmet for underwater semiautomatic (hand-held) welding.

One green LED is used to indicate the execution of the program. If the program is normally executed, it will be turned on in one spinning cycle and off in the next cycle. So if it flashes at half the spinning frequency, the program is executing normally.

Seven LEDs are used to indicate the arc-joint deviation. The central one is green and is always on. The others are red color. When the arc is at the right side of joint center, the right side LEDs will light. When the deviation is small, only the one nearest to center is on, if the deviation is at moderate level, two will be on; if deviation is big, all three will light. The thresholds are set in the program based on experiment data.

Table 4.1 LED display logic

Arc Position	LED6	LED5	LED4	LED3	LED2	LED1	LED0
Far Left	☼	☼	☼	☼			
Mid-Left		☼	☼	☼			
Near Left			☼	☼			
Center				☼			
Near Right				☼	☼		
Mid-Right				☼	☼	☼	
Far Right				☼	☼	☼	☼

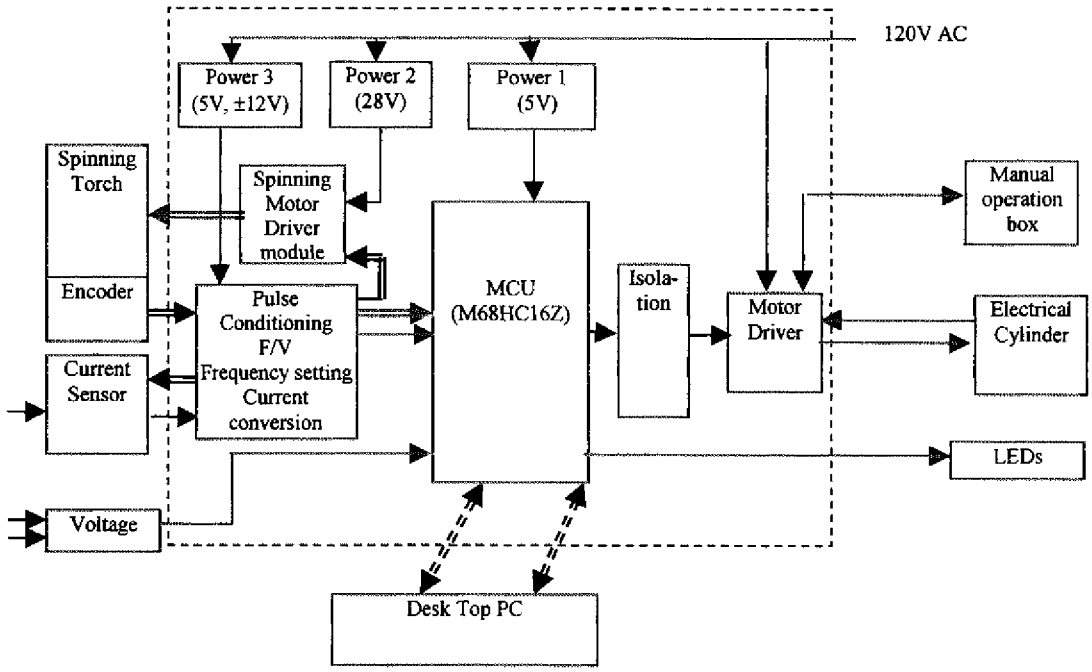

Figure 4.1 Microcontroller based system block diagram. The desktop PC is used for debug only.

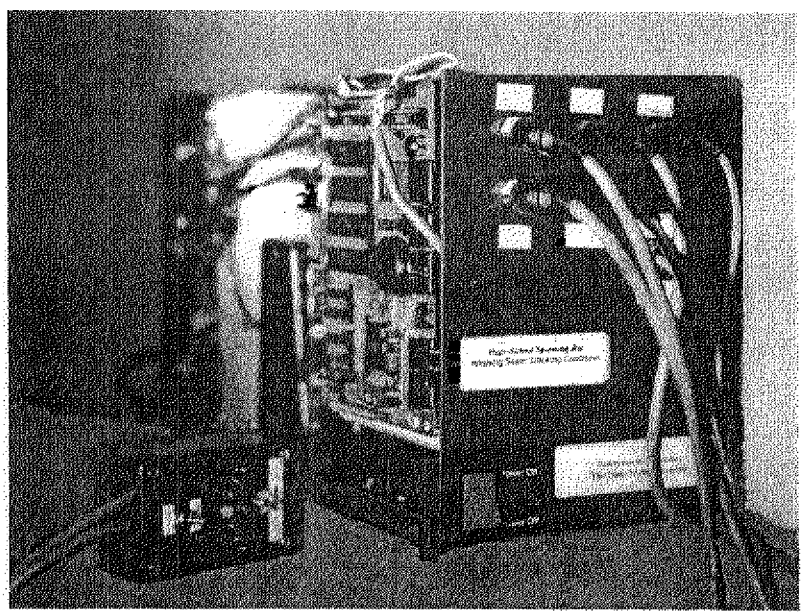

Figure4.2 Picture of the microcontroller based seam-tracking controller

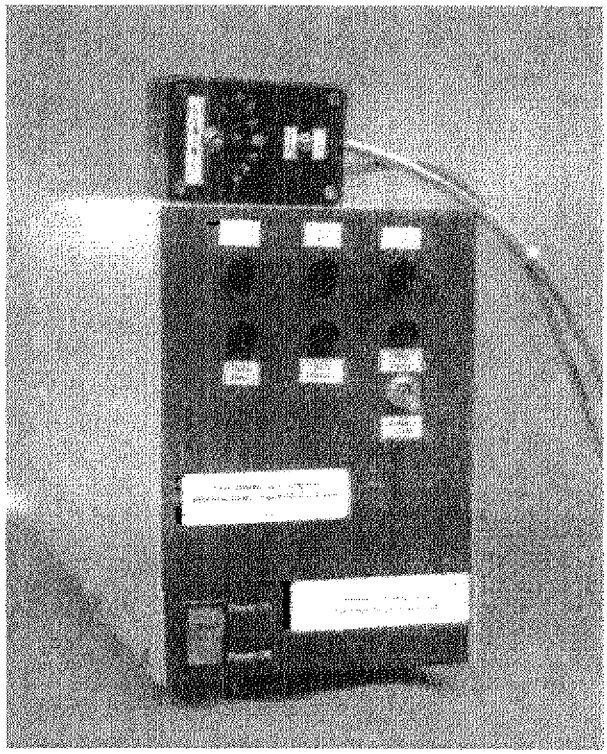

Figure 4.3 Appearance of the seam-tracking controller

4.3 M68HC16 microcontroller Software Development

The MCU system function and control algorithm is the same as the PC based system (section 3.4). The welding current is sampled synchronously with the arc positioning codes. Then the waveform is filtered and according to the waveform, the torch-joint deviation is calculated. The microcontroller outputs the deviation signal on the display and sends the control signal to the actuator driving circuit to correct the torch position.

As the differences of hardware resource and software platform, the coding strategy is much different from the PC based system. Motorola 16-bit assembly language was used to produce the program. The coding deals with the hardware directly. Usually the codes made this way can reach the fastest speed and smallest coding space.

Figure 4.4 is the flowchart of the program. As many real-time feedback control programs, the main program, after initialization, goes to a "dead-loop" waiting for interrupts or condition to call other subroutines. When the marking pulse (the start of a spinning circle) or indexing pulse

(corresponding to the 64 positions of the encoder) comes, the CPU response and jumps to the interrupt service routines.

In the marking pulse service routine, the MCU determines whether it is time to update the arc-joint deviation calculation and make a new adjustment of the torch position (a "adjusting cycle") or not (still time to sample). As the spinning frequency is around 20Hz, the updating is made each 4~5 scans, resulting in an adjustment frequency of 5~4Hz. This rate has been proved appropriate by experiments (discussed in next chapter). In the adjusting cycle, a flag was set to enable the main program to call the processing subroutine. In a sampling cycle, the data storing base address is set according to the cycle sequence and phase shift. Each scan cycle needs a "page" of memory to store the 64 data, and the total pages required equals to the numbers of spinning cycles in a adjusting period less one.

In the indexing pulse service routine, the arc current at the current position is sampled. The time interval in two indexing pulses is enough to finish the multi-cycle average of one arc position.

In the processing subroutine, the watchdog is reset first. As the adjustment period may be set to 0.2~0.4 second (2.5~5Hz), the watchdog activation time is set to 1 second. For any reason the watchdog is not reset with one second, it will cause the whole system reset, and the program executes from the very beginning again. This ensures the system not "hang-up" for long time. For example, when several marking pulses are lost due to electric interference, the adjusting will not be updated, and the actuator may keep running at a wrong direction or speed. The MCU reset will initialized the whole system, include clear output. In the case of marking pulse lost, the program execution status LED indicator will also show the error.

Then the data resulted from multi cycle average is further filtered with the sliding window average. The M68HC16 MCU has a set of powerful signal processing instructions that make the program of calculating the arc-joint deviation by correlation method simple. Once the torch-joint deviation is found, the actuator can be controlled to move left or right at an appropriate speed according the current, history, and trend of the deviation. If the actuator needs to move to left, PWM channel A is set to a duty cycle proportional to the required speed, channel B is set to 0. When it needs to move to right, PWM A is set to 0 duty cycle, channel B is set to required value.

With the experiment-based thresholds, the LED indicators are controlled to light as table 4.1.

In case the indexing pulses are lost, the processing program will use the "old" data to calculate the deviation. In order to avoid such misuse, before returning to the main program, the original data used in the subroutine are cleared (set to zeros). In the next adjusting cycle, the zero data results in the calculated deviation being zero, thus the actuator will stop rather than keep running at wrong speed or direction.

The control program is listed in appendix.

The program discussed above is the final codes burned into the EEPROM on the controller board. This is one of reasons that a microcontroller has stronger ability to resist electric/magnetic disturbance than PC in which the program is executed in RAM.

At the developing stage, RAM version codes are programmed first for debug and modifying. With support of developing software, a desktop PC is used as the terminals to reach the MCU contents. An In-Circuit-Debug (ICD) cable connects the PC and the MCU board.

When the program is proved functioning well, it is transfer to the ROM version and permanently programmed in the EEPROM chips. The PC can also used as a real-time terminal of the MCU through serial communication to accept/display information.

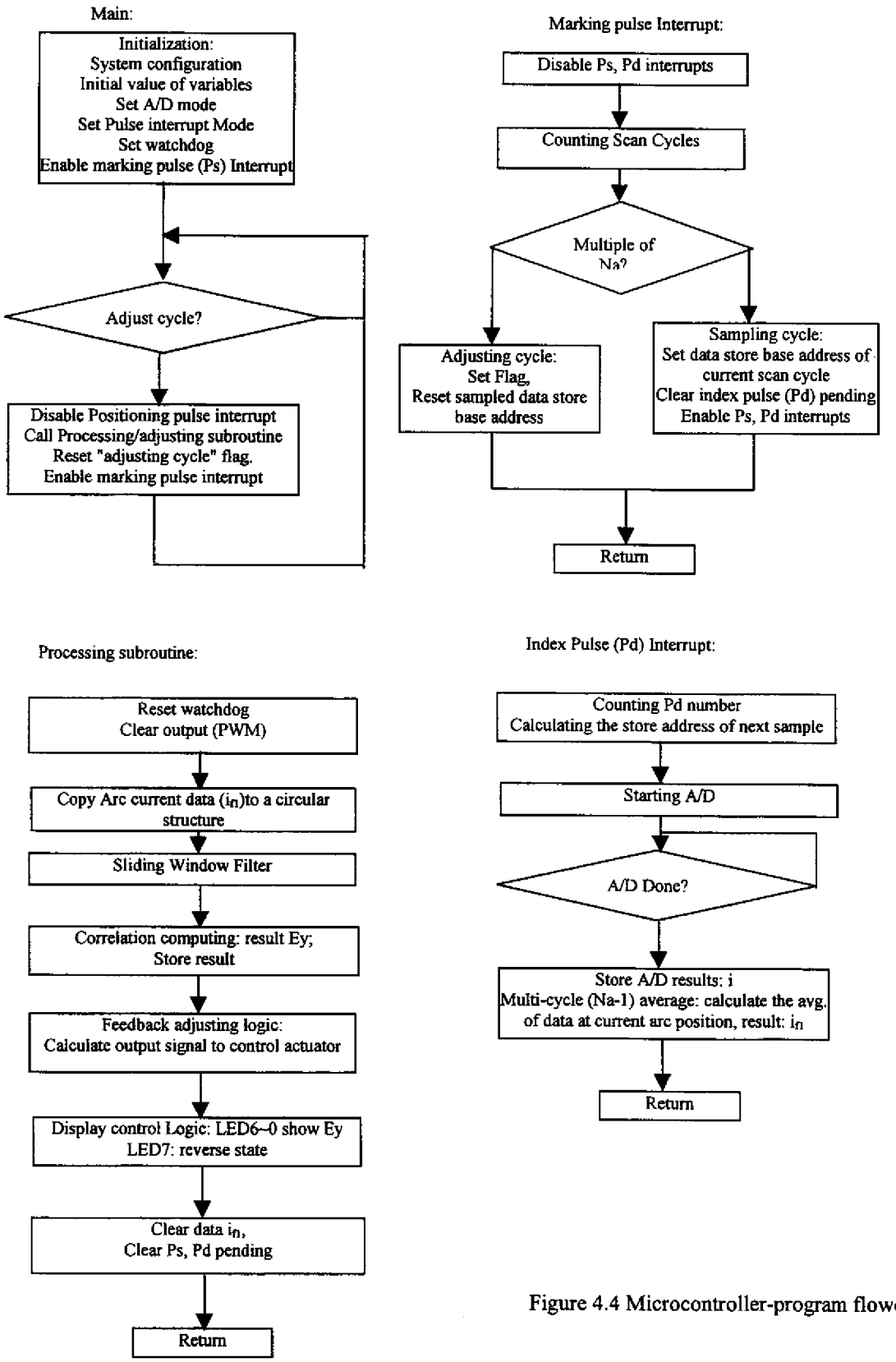

Figure 4.4 Microcontroller-program flowchart

CHAPTER 5

WELDING TESTS AND EVALUATION

5.1 Tests and Results on Seam Tracking

5.1.1 Arc Sensor Output

According to the definition of "sensor", the arc sensor is the device to detect the torch-joint deviation. Thus it consists the spinning torch and the MCU processor with the part of software calculating the deviation, as shown in Figure 3.6. Experiments were carried out to test the input-output properties. In these tests the arc spinning frequency was at the range of 18~25Hz, the high sensitivity range.

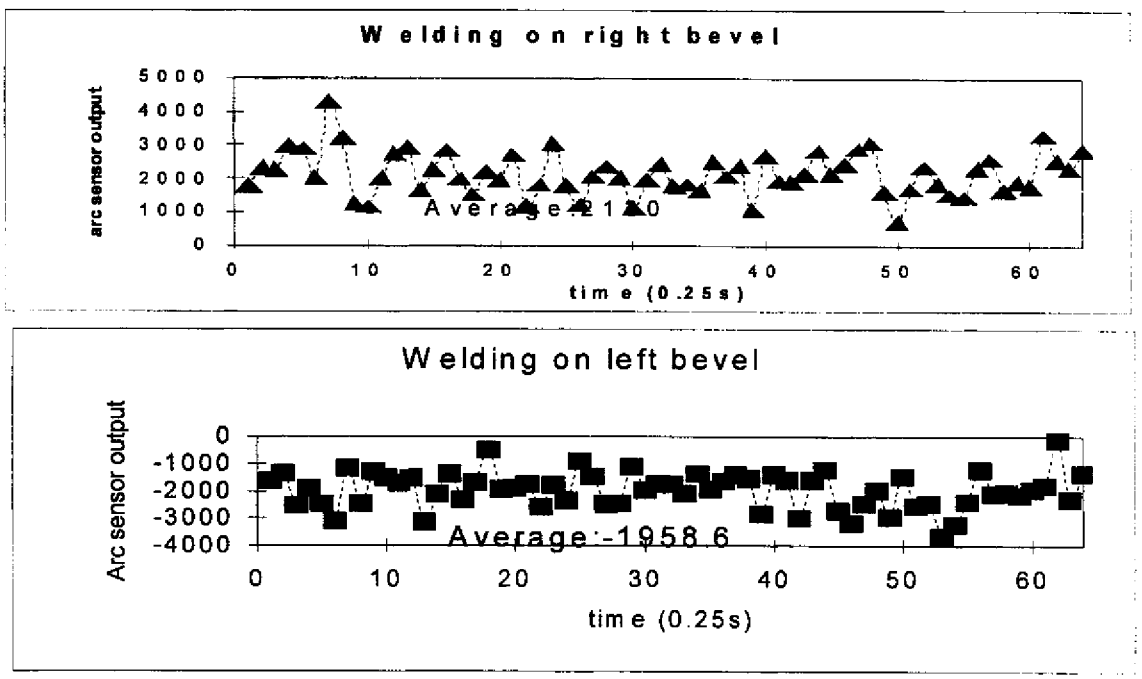

Figure 5.1 Arc sensor output when torch deviate to one side of groove (a) to right side, (b) to left side. Y-axis unit is arbitrary

The first set of tests was done as bead-on-plate welds, with left side or right side of the plates raised at an angle of 30°. It is similar to the case where torch is at one bevel of the welding groove. Figure 5.1 shows the processor calculated deviation data.

Figure 5.1 (a) shows the detected deviation presented in digit, when the torch completely deviated to left bevel. Although it varies a lot (from 1000 to 3000), considering its updating rate is only 0.25 second, the variation can be smoothed with a filter easily. In actual feedback tracking, the inertia of the actuator is itself a low-pass filter. The average value is 2130.

Figure 5.1(b) shows the sensor output when torch at the right bevel of the groove. The average value is -1959. The results show the agreement between analysis and test.

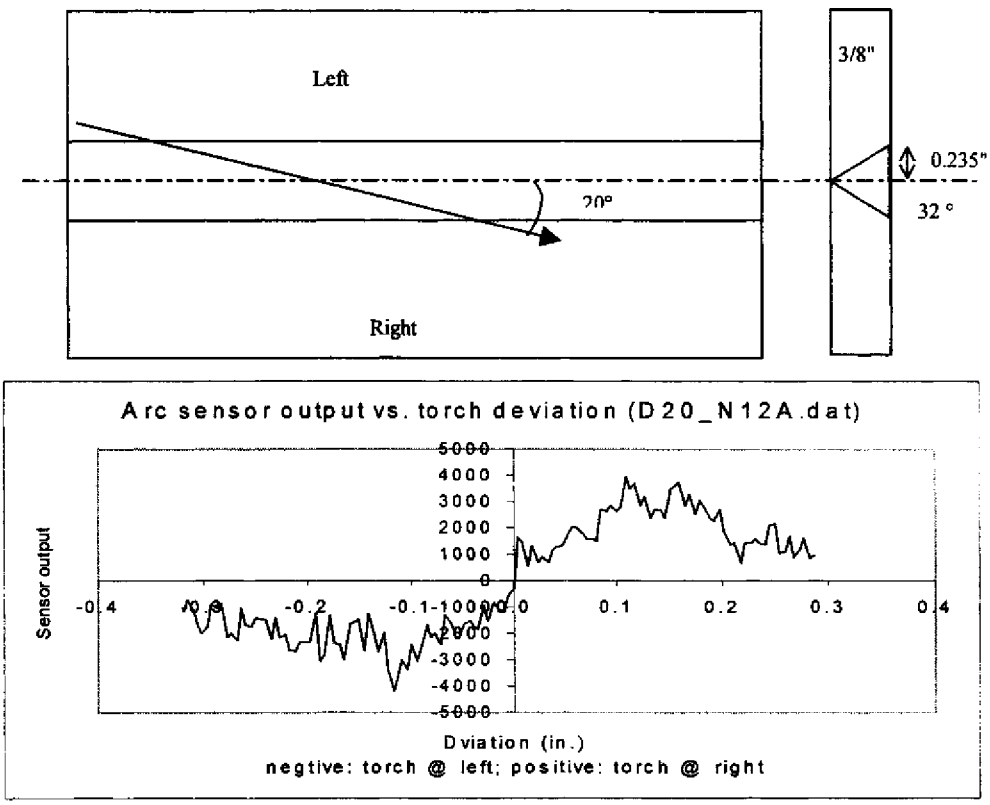

Figure 5.2 Arc sensor output when welding on V-groove joint (a) setting, (b) data

The second set of tests was made on V-groove joints without feedback control. By placing the joint centerline at an angle to welding direction, the torch-joint deviation changes linearly from left to right as shown in Figure 5.2(a). The arc sensor output is shown in Figure 5.2(b). At the beginning and end parts, the arc was burning almost on the flat surface of plate, so sensor output is very small. Between the effective range (±0.1 inch) the linearity is good.

5.1.2 Welding Seam Tracking

Tests on seam tracking were performed both in-air and underwater. One type of samples were straight-line joints placed at an angle of 5~12° to the welding direction. The other type was broken-line or curved joints. Figure 5.3 is the pictures of the welding samples.

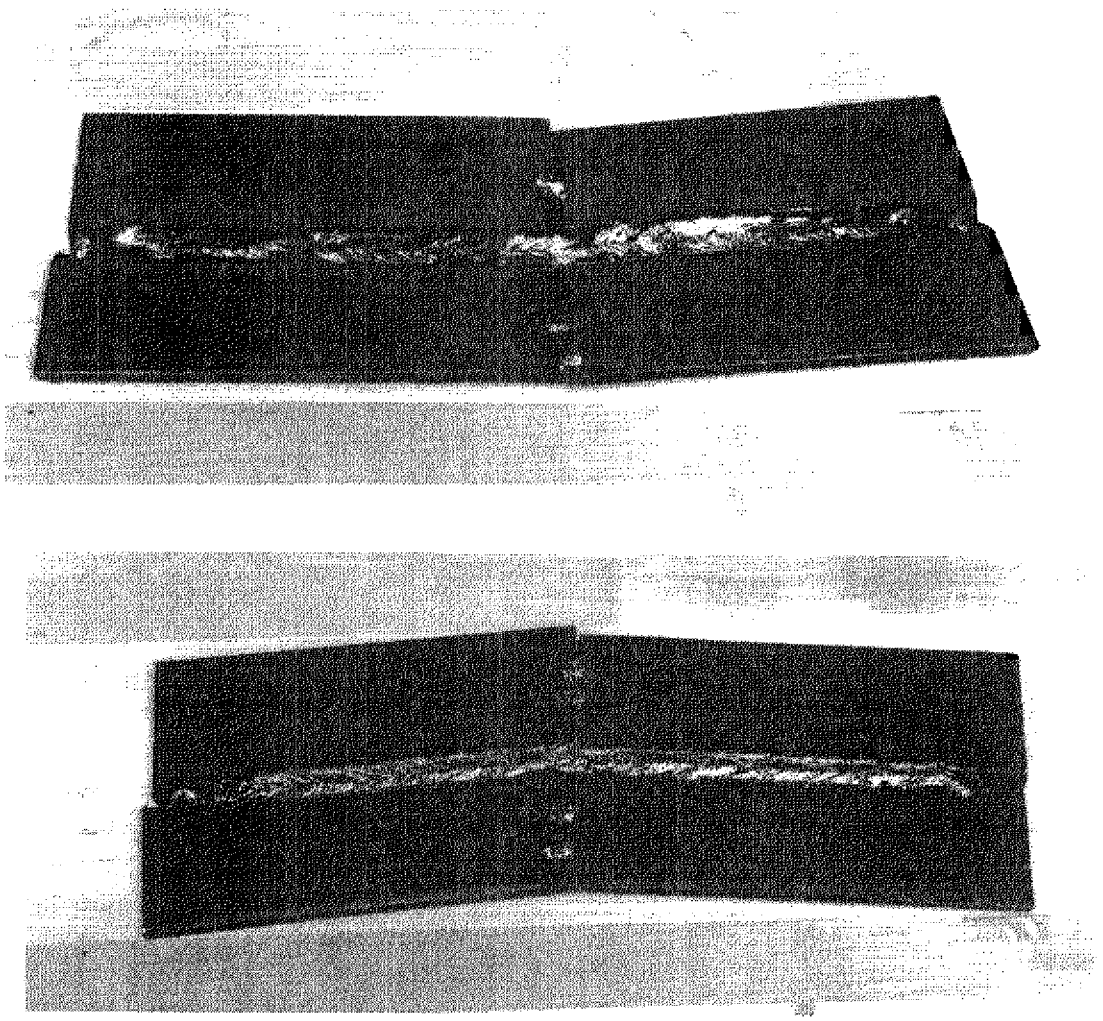

Figure 5.3 Sample of welding seam tracking with spinning arc sensor. Upper : underwater welding, bottom: in-air welding.

The welding parameters:

In-air welding: current 150~200A; voltage: 22~24V; travel speed 255mm/min (10 ipm) ; no external shielding gas.

Underwater welding: current: 180~200A; Voltage: 29~32V; travel speed: 225mm/min (10 ipm); shielding gas: 20cfh air.

The arc spinning speed is 20Hz for in-air welding and 25Hz for underwater welding. Spinning diameter: 4mm. Adjusting rate: once per 5 spinning cycles.

5.2 Evaluation of Weld Quality

In this project, the measures for protection arc and weld from the water environment are based on the results of the previous research. A contoured flexible shroud covered the critical welding area gives good protection. As the welding material (type 308L flux-cored wire and A36 base metal) and other conditions (water depth, plate thickness, heat input, travel speed) are the same as in the previous project except the arc is spinning when welding, the cooling condition and weld microstructure are expected to be the same. The spinning arc may have some effect on metal transfer and weld appearance when welding parameters are not set properly. The eccentric force may cause short-circuit metal transfer changes to globular transfer when CTWD is too large or arc too long, and cause spatters. But the authors' research of in-air spinning arc showed that when the spinning diameter is small as used in this project (less than 4mm), the spinning of arc has a negligible effect.

5.2.1 Weld Cooling Rate

The weld cooling rates were measured by thermocouples attached in backside blind holes. The bottoms of the holes were at the welding fusion line. Figure 5.4 is a typical record of temperature change versus time. The welding parameters are voltage 31V, current 210A, travel speed 10ipm (254mm/min), heat input 1.5MJ/m. The cooling time from 800°C to 500°C ($T_{8/5}$) is 7.3 seconds. This cooling rate is very favorable for microstructures (Bainite and Ferrite) with better toughness than Martensite that resulted from quenching.

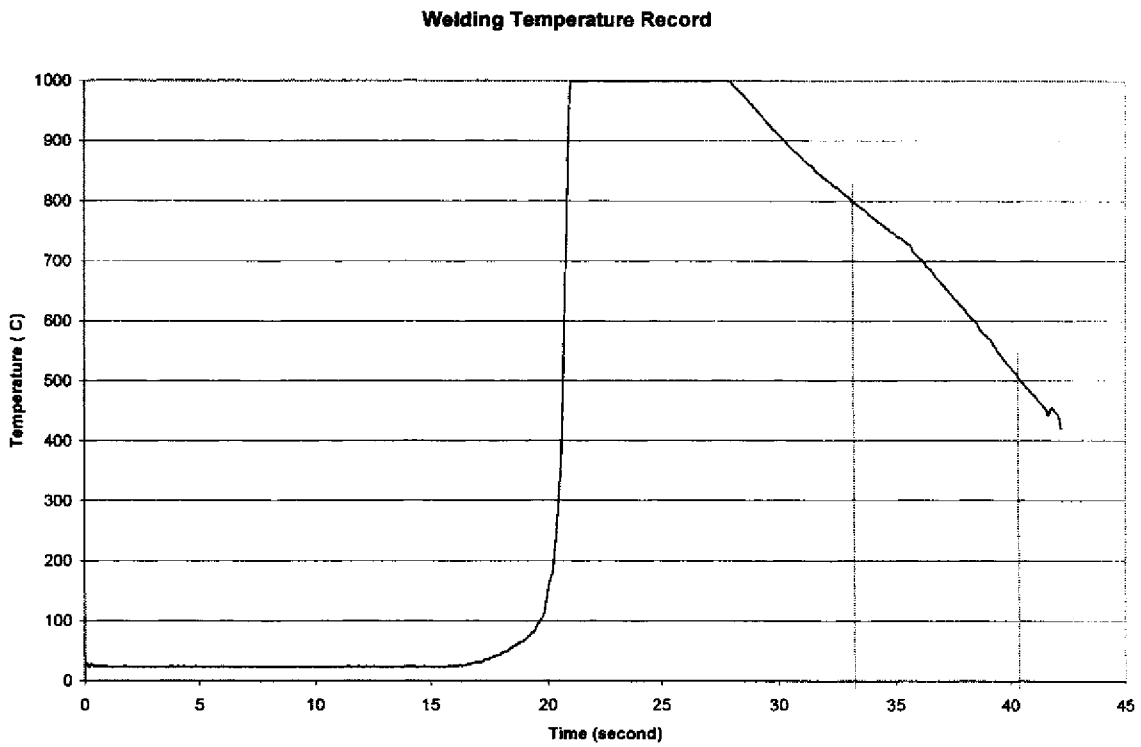

Figure 5.4 Fusion line temperature record, the measuring instrument is saturated at 1000°C.

5.2.2 Microstructures of Weld Metal and Heat Effected Zone

Microstructures of weld and heat affected zone metal were evaluated with metallographic techniques. Figure 5.5 through 5.8 are microstructure pictures of typical weld and HAZ metals.

The weld metal composition was determined by the composition of the filler metal (308 stainless steel), the composition of the base metal (A36 mild steel), and the weld metal dilution. The dilution was a measure of the amount of base metal that was melted in relation to the amount of weld metal melted and is reported in percent. The underwater wet welds were low dilution welds ranging between 20 and 35 per cent, depending on the heat input. The microstructure of weld metal is determined by its composition and the cooling procedure. With a cooling rate ($T_{8/5}$) of about 7 second, the structure is mostly Austenite and some Ferrite.

The base metal is hot rolled plate. The carbon equivalent near 0.4%. With the composition given, the microstructures of the HAZ are determined by the cooling rate only. With the slow cooling rate about 7 seconds, little Martensite is formed, the near HAZ has structures with good toughness.

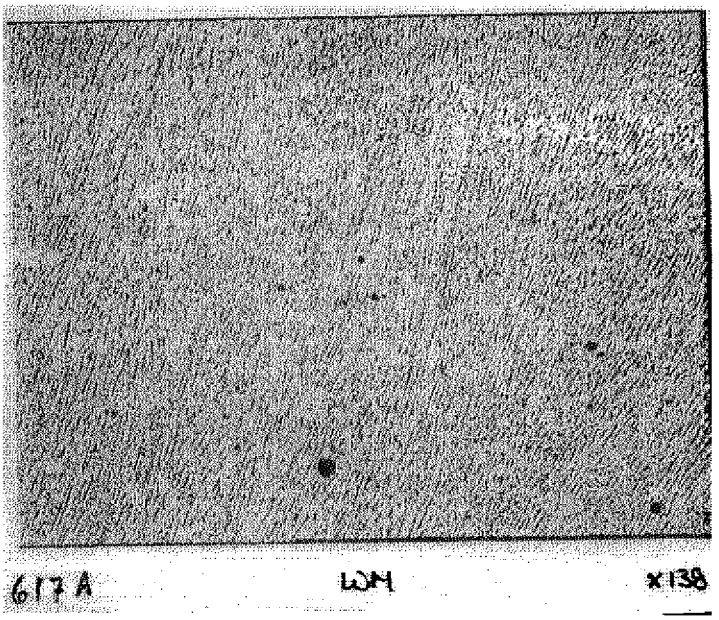

Figure 5.5 All-weld-metal microstructures (picture has no secondary magnification).

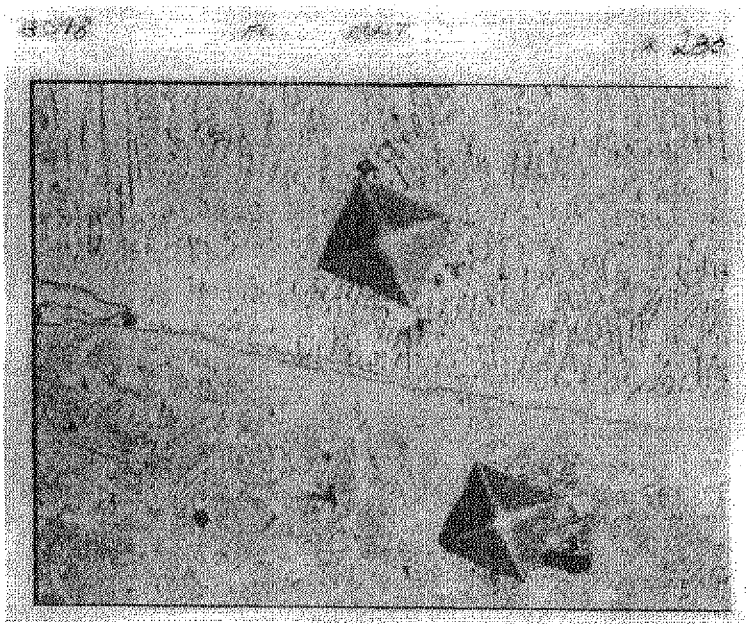

Figure 5.6 Microstructures at fusion line near joint root. The diamond is micro hardness test spot. The upper part is weld metal, lower part is HAZ. (Picture has no secondary magnification).

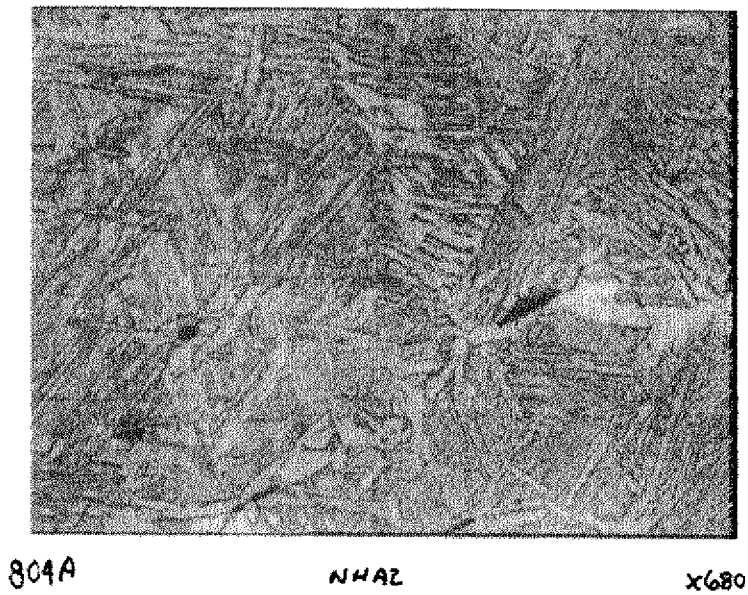

Figure 5.7 Near HAZ microstructures (picture has no secondary magnification).

5.2.3 Meachnical Properties Tests

Weld quality of underwater welds is normally assessed in accordance with the ANSI/AWS D 3.6 American National Standard, *Specification for Underwater Welding*. This standard defines four different weld quality classes: Class A, Class B, Class C, and Class O. Class A welds, the highest quality underwater welds, are "intended to be suitable for structural applications". The tests were aimed at qualifying class A weld.

The welds were done in approximately 8" of fresh water in the small test tank with mechanized system. The welds were Flux Cored Arc Welded 308L Stainless Steel with A-36 base metal. Base metal thickness is 3/8 inch.

Several test coupons were welded for mechanical properties test. Not all the mechanical tests required by Code D3.6 for Class A were performed, but the typical bending test that addresses the main problem in underwater welding, that is, brittleness,

was conducted. Face and root bends have reached 180° angle at 2T-radius test, meeting Class A bending test requirement. Figure 5.8 shows the bending test results.

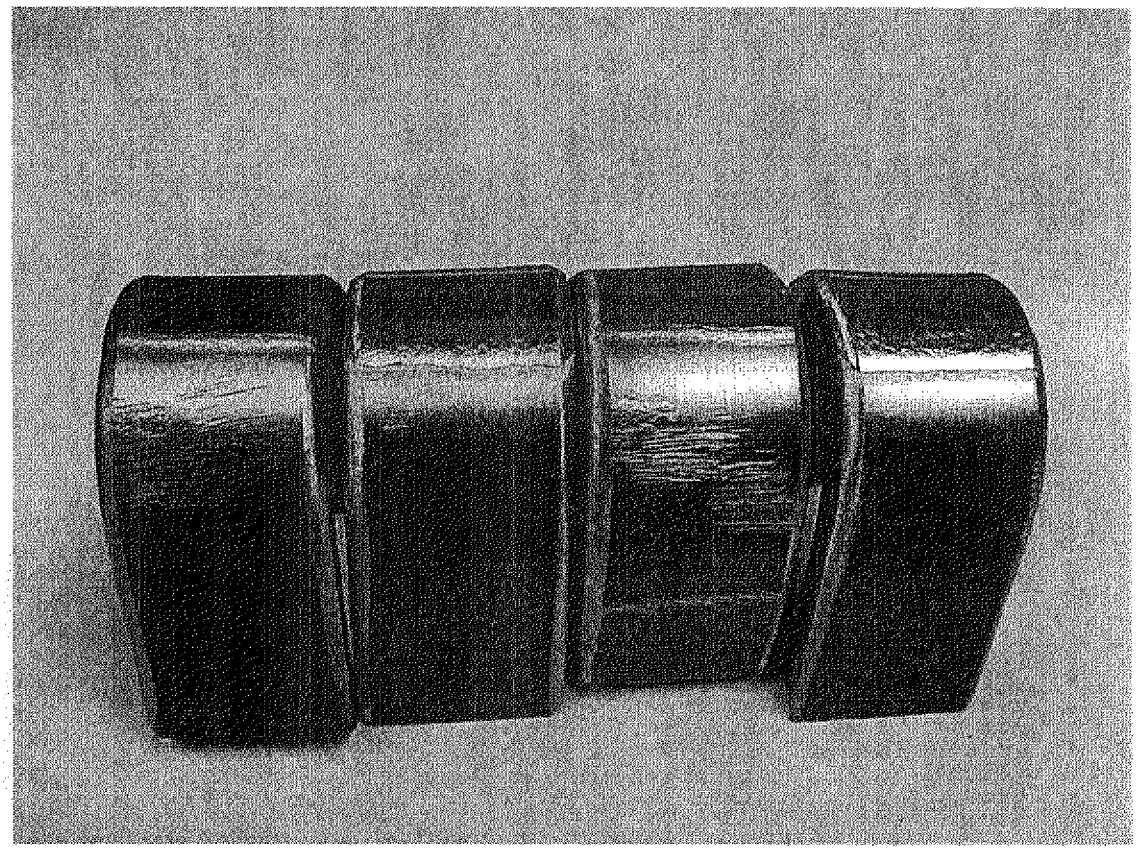

Figure 5.8 Photograph of Face and root bending specimen

CHAPTER 6

CONCLUSIONS

Conclusions

With spinning arc as the sensor for welding joint seam tracking, the harsh environment of arc and water do not interfere the functioning of the system. While many other types of sensors may be affected by the high temperature, spatter, fume, strong arc light and magnetic field of the welding current, arc sensor works well as long as the arc itself is stable. It could be one of the best choices for underwater welding seam tracking or operation guidance.

The static and dynamic models of arc-power supply system were studied theoretically, by simulation and experiments. For GMAW and FCAW, the arc current decreases linearly with increase of contact tip to work distance (CTWD) in the normal welding current range. The ratio is 1.5~3.5A/mm determined by arc type and material. When the torch scans the joint groove at high frequency, with the same CTWD change, the arc current changes greater than at static state. The high-gain range is 15~35 Hz, also depending on arc type, material and base parameters (set point). The dynamic gain may be as much as 3~5 times of the static gain.

In order to reach high sensitivity, high speed spinning arc sensor is preferable. A hollow-shaft motor direct driven circular swing mechanism was developed to realize high speed spinning of the arc. A rotary encoder was embedded in this mechanism to detect spinning position and speed. Speed feed back control was adopted to ensure smooth rotation over a large speed range. This torch ensures no feed wire twisting and can be sealed directly with nibbles or sealant. It can either be mounted on a mechanized welding carriage or manually held by a diver/welder.

A PC based prototype was developed for arc sensor signal acquisition, processing, feedback control and guidance signal generation. With this system, the arc sensor data were collected for arc sensor model analysis and set up a database for determining control parameters. The system can control a motorized cylinder to adjust the torch position to track the joint center

through feedback control algorithm, and output signals to an LED array to show the torch position with respect to the joint center.

A commercial demo system was developed through integration of a Motorola M68HC16Z microcontroller board, spinning torch control, signal interfacing board, and tracking motor control. This system was packed and enclosed in an instrument case, could be served as a product design prototype. Compared to the PC system, it has a small size, low cost, and stronger resistance to electrical interference. This system can be used for both automatic seam tracking in mechanized welding and semiautomatic diving welding.

Welding experiments were performed with both systems. The contoured shroud was used to protect the arc and weld from water intrusion. For the welding process and material used in this project, the arc spinning speed set at 20~25Hz, with adjusting rate of 4~5Hz is suitable. With the mechanized feedback control system, seam tracking sample tests were produced with satisfactory tracking results. With semiautomatic (hand-held) welding, the visual signals from the controller can give the guidance for the welder to track the joint. But some practice may be need for welders to get acquainted with the indications and develop corresponding eye-hand coordination.

Welding with 3/8" mild steel and 308L stainless steel filler wire, and the contoured shroud, the weld cooling rate is retarded so that the welds have structures with good toughness. The face and root bend tests reached 180°, showing the toughness meets the requirements of the Underwater Welding Code D3.6 Class A weld.

By integration of the developed shielding method and joint tracking technique, underwater wet welding with flux-cored stainless wire on mild steel structure could obtain more application and benefits the industries and the nation.

REFERENCES

1. Tsai, Chon L. and Masubuchi K., *Mechanisms of rapid cooling in underwater welding.* Applied Ocean Research, Vol. 1, No.2, 1979.
2. Tsai, Chon L. et al. *Development of an Underwater SMAW Electrode for Improved Fatigue Strength in Wet Welded Joints.* Ohio's Thomas A. Edison Program, Edison Seed Development Fund Technical Report, The Ohio State University, Columbus Ohio, June 1991.
3. Tsai, Chon L, and Jiang, C. H., *Verification and Dissemination of the Required Engineering DataBase for the New Underwater, Flux-Coated Welding Electrode in Commercial Applications.* An NCRI Final Report, OSU RF Project # 727962. Ohio State University, Columbus, OH 43210, Dec 95.
4. Tsai, Chon L., et. al. *Engineering Assessment of Weld Joint Design for Underwater "Wet" Welding.* Navy Joining Center final report. The Ohio State University, March 1995.
5. American Welding Society. *Specification for Underwater Welding.* AWS D3.6 - 93, American Welding Society, Inc., Miami, FL 33135, 1993.
6. Tsai, Chon L., Jiang, C. H., and Kang, D., *Development of a Smart Underwater "Wet" Welding Process,* Ohio Sea Grant College Program, The Ohio State University, Final Report, October 31, 1996.
7. Tsai, Chon L., Liao, B. J., *Control algorithm for underwater wet flux-cored arc welding process.* Ohio Sea Grant College Program, The Ohio State University, Final Report, August 1998.
8. Lancaster, J. F., *The Physics of Welding*, Pergamon Press, 1986
9. Nomura, H., *Sensors and Control Systems in Arc Welding*, Chapman & Hall, 1994
10. Halmoy, E. and Brotan H., *Dynamic Response of the Melting Rate*, IIW publication session Bratislava, Aug 1979.
11. Pan, J. and Liao, B. J., *Fuzzy Control of Multi-freedom Welding Machine*, China Welding (English version), 1993(2).
12. Liao, B. J., *Automatic Seam Tracking of Curved-line Welding Joints*, Chinese Mechanical Engineering, 1994(2).
13. Lesnewich, A., *Control of Melting Rate and Metal Transfer in Gas Shielded Metal Arc Welding*, Welding J., 37(8) &37(9), 1958

APPENDICES

A. Spinning Arc Joint Seam Tracking Program for PC Based System (Borland C Codes)

```
/* This program used for spinning arc sensor based seam tracking */
/* Modified 99/9/15, "Sin999A.C", rotation direction: counterclockwise,
   3 o'clock start, isolated pulse input */
/* Arc current--
        --Ch10: hallsensor: 500A/100mA/5V; module: (-5V~5V)/(0~5V)
      PreADamp: 5V/10V; A/D: 10V/4096;
      Total:  0~500A-->2048~4095 for Ch10 */
/* No rotate speed counting */

/* C INCLUDE FILES */
#include "stdio.h"
#include "stdlib.h"
#include "conio.h"
#include "dasdecl.h"
#include "das1600.h"
#include "graphics.h"
#include "math.h"
#include "dos.h"

/* LOCAL VARIABLES */
  DWORD    hDrv1600;       /* Driver Handle */
  DWORD    hDev1600;       /* Device Handle */
  DWORD    hFrameAD1600;   /* A/D Frame Handle */
  short    nErr;           /* Function return error flag */
  int      anDataBufA[4096]; /* data buffer */
  int              anDataBufB[4096];  /*32 circle max */
  DWORD    dwSamples ;             /* Number of samples to aquire */
  short    nStatus;        /* Used to monitor data transfers */
  DWORD    dwTransfers;    /* Used to monitor data transfers */
```

```
  DWORD     dwOUTval;
  DWORD     dwINPval;
  WORD          CtrDataL,CtrDataH;
  int           CtrVal,CtrVal_1;
  char far *szErrMsg;       /* Pointer to error message */
  char      in_com;
  FILE      *out1,*out2,*out3;
  int       file_write1=0,file_write2=0,file_write3=0,manual_move=0;
  char      file_name1[20],file_name2[20],file_name3[20];

  float   curatio=4.096; //0~500A-->2048~4096
  float   fr,fa;
  int           N=64,Nsamp,Nadj=4;
  float   Current,Voltage,Ana_in,Ana_out;
  int     Digit_I;
  float   Total_I,real_I,real_If[64];
  int           PAGE,Cadj;        // Cadj: Adjusting counter
  float   COS[64],Deviate=0,Deviate_1=0,Kadj=0.01;
  int           Phi_freq=0,Phi_startP=0; //modified 8/24:Phi=5
  float   pulse_number;

  int     x[128],yf[128],yr[128],drawratio=3;
  int     driver,mode;
  int     i,j,mbufindx;


  int           N1;       // C/T divisors
  short   N1H,N1L,N2L=8;

void DisplayError(char *szFuncName, short nErr);

/* BEGIN MAIN MODULE */
main()
{  float start_time,now_time,time_pass;
   float ptime,ptime_1,period;
   short time_read=0;
   struct  time real_time;

   printf("Set torch electrod spinning speed 20-30Hz and turn on it!\n");
```

```
printf("Pease set adjusting rate (per 4~12 revolve): Nadj=");
scanf("%d",&Nadj);
if (Nadj<2) Nadj=2;
if (Nadj>16) Nadj=16;
Nsamp=(Nadj-1)*N;  // sample number in one adjust period
dwSamples=(long) Nsamp;

printf("Please set tracking control loop gain (0.005-0.05):Kadj=");
scanf("%f",&Kadj);

printf("Do you want to write the currentwave to a file? ( y/n )\n");
in_com=getch();
if ( (in_com=='y') || (in_com=='Y') )
{ file_write1=1;
 printf("Enter saving filename\n");
 scanf("%s",file_name1);
 printf("%s\n",file_name1);
 out1=fopen(file_name1,"wt");
}

printf("Do you want to write the filtered waveform to a file? ( y/n )\n");
in_com=getch();
if ( (in_com=='y') || (in_com=='Y') )
{ file_write2=1;
 printf("Enter saving filename\n");
 scanf("%s",file_name2);
 printf("%s\n",file_name2);
 out2=fopen(file_name2,"wt");
}

printf("Do you want to write the result to a file? ( y/n )\n");
in_com=getch();
if ( (in_com=='y') || (in_com=='Y') )
{ file_write3=1;
 printf("Enter saving filename\n");
 scanf("%s",file_name3);
 printf("%s\n",file_name3);
 out3=fopen(file_name3,"wt");
}
```

```
in_com='0';

        drawratio=3;  // drwing ratio
        driver=DETECT;
        initgraph(&driver,&mode,"");

        setlinestyle(SOLID_LINE,1,1);

        setcolor(YELLOW);
        rectangle(127,128,385,384);

        outtextxy(20,200,"Arc Current");
        setcolor(RED);
        rectangle(254,136,258,176);


 if (K_OpenDriver("DAS1600", "das1600.cfg", &hDrv1600)!= 0)
 {      putch (7); printf( " Error %X during K_OpenDriver " ) ;     exit(1); }

 if ( K_GetDevHandle(hDrv1600, 0, &hDev1600) != 0)
 {      putch (7); printf( " Error %X during K_GetDevHandle ") ; exit(1); }

 DAS1600_8254Control(0, 0x30); //C/T0 as counter
 DAS1600_8254SetClk0(0,1);   // use external clk
 DAS1600_8254SetCounter(0,0,0x00);
 DAS1600_8254SetCounter(0,0,0x00);
 CtrVal_1=0;

//stop actuator
 dwOUTval =  2048;
 dwOUTval = ( dwOUTval << 4 ) & 0xfff0;
 if ( (nErr = K_DAWrite(hDev1600, 0, dwOUTval)) != 0)
 {
        putch (7); printf( "Error %X during Digital Output.", nErr );
        exit(1);
 }
 //initialize Counter0 as index pulse(Pd) counter


/* Initialize Intrrupt mode A/D*/
```

```
  if ( (nErr = K_GetADFrame( hDev1600, &hFrameAD1600))!= 0) //int_AD initia
   {      DisplayError("K_GetADFrame", nErr);exit(1);   }

  if ((nErr=K_SetChn(hFrameAD1600,10))!=0) /*set AD ch10: hall Arc Current*/
   { DisplayError("K_SetChn",nErr);  exit(1);    }
  if ((nErr=K_SetG(hFrameAD1600,1))!=0)   /*set gain=1: *2 */
   { DisplayError("K_SetG",nErr);  exit(1);   }

/* SPECIFY  outer pacer CLOCK : pulse "Pd" on pin Xpclk */
  if ((nErr = K_SetClk(hFrameAD1600, 1)) != 0)
  {       DisplayError("K_SetClk", nErr);          exit(1); }

/*Specify outer digital triger (pulse "Ps" on pin Xtrig)*/
  if ((nErr= K_SetTrig(hFrameAD1600,1))!=0)
  {       DisplayError("K_SetTrig",nErr);exit(1);             }
/* use this  setting: digital positive Edge triger*/
  if ((nErr=K_SetDITrig(hFrameAD1600,0,0,0))!=0 )
  {       DisplayError("K_SetDITrig",nErr);exit(1);}
// Interupt A/D set finished

  for(j=0;j<32;j++)
  {
   for (i=0;i<N;i++)
   { anDataBufB[N*j+i]=2048; // Clear first buffPAGE
   }
  }

  for (i=0;i<N;i++)      //make cosin fuction table
  {COS[i]=cos(2*3.1415926*((float)(i+Phi_freq)/64.0));}

  for (i=0;i<N/2;i++)  //front/rear half rotating circle, x step up from right to left
         { x[i]=384-8*i;
         }


/* START ACQUISITION */

  printf("\n Press ENTER key  to begin control");
  printf("\n Press SPACEBAR  key to stop control\n\n");
```

```
wait: while(!kbhit()) {  }; //waiting start Key
  in_com=getch();
  if (in_com=='\x20') {goto stop;}
  if (in_com=='\x0d') {goto start;}
  goto wait;


start: PAGE=-1; Cadj=0;

 do                    //main circulation
 {

  dwTransfers=0;
  PAGE=-PAGE;
  Deviate_1=Deviate;Deviate=0;Total_I=0;

  switch(PAGE)      //start A/D, read data buffer to array, wave avg.
  { case 1:
              { K_SetBuf (hFrameAD1600, anDataBufA, dwSamples);
                K_IntStart (hFrameAD1600);  //starting sample for pageA

                if (Cadj<1) goto waitingADEOC;

                for (i=0;i<N;i++)     //point index
                { real_If[i]=0;
                      for (j=0;j<Nadj-1;j++)   //circle index
                       { mbufindx=(N*j+i+Phi_startP+Nsamp)%Nsamp;
                         dwINPval = ( anDataBufB[mbufindx] >> 4) & 0X0FFF;
                         if (dwINPval==0) {dwINPval=4096;}
                         Digit_I = dwINPval-2048; //current:0~500A-->2048~4095
                         real_I=Digit_I/curatio;
                         real_If[i]=real_If[i]+real_I;
                         if (file_write1 == 1) {fprintf(out1,"%4.1f\n",real_I); }
                       } //loop j end

                      real_If[i]=real_If[i]/(Nadj-1);
                      if (file_write2 == 1) { fprintf(out2,"%4.1f\n",real_If[i]); }
                      Deviate=Deviate+COS[i]*real_If[i];
                      Total_I=Total_I+real_If[i];
                } //end i loop
```

```
            } break;//end case 1

  case -1:{ K_SetBuf (hFrameAD1600, anDataBufB, dwSamples);
            K_IntStart (hFrameAD1600);

            for (i=0;i<N;i++)
            { real_If[i]=0;
                  for (j=0;j<Nadj-1;j++)
                  { mbufindx=(N*j+i+Phi_startP+Nsamp)%Nsamp;
                    dwINPval = ( anDataBufA[mbufindx] >> 4) & 0X0FFF;
                    if (dwINPval==0) {dwINPval=4096;}
                    Digit_I = dwINPval-2048; //current:0~500A-->2048~3072
                    real_I=Digit_I/curatio;
                    real_If[i]=real_If[i]+real_I ;
                    if (file_write1 == 1) { fprintf(out1,"%4.1f\n",real_I);}
                  }
                 real_If[i]=real_If[i]/(Nadj-1);
                 if (file_write2 == 1)  {fprintf(out2,"%4.1f\n",real_If[i]);}
                 Deviate=Deviate+COS[i]*real_If[i];
                 Total_I=Total_I+real_If[i];
            }
           } break;  //end case-1
  default:break;
  }; //end switch

           Deviate=0.75*Deviate+0.25*Deviate_1;
           Current=Total_I/N;

// display graph:
/*         for(i=0;i<32;i++)
            { putpixel(x[i],yf[i],BLACK); //front half circle
                  yf[i]=384-real_If[i]/drawratio;
                  putpixel(x[i],yf[i],YELLOW);

                  putpixel(x[i],yr[i],BLACK); //rear 1/2 circle
                  yr[i]=384-real_If[63-i]/drawratio;
                  putpixel(x[i],yr[i],GREEN);
            }
*/
```

```
//Actuator moving control
Ana_out=-Kadj*0.1*Deviate; //dev>0 means RH, move to left,
                           //retrac, servo given minus
if(Ana_out>9.5) {Ana_out=9.5;}
if(Ana_out<-9.5) {Ana_out=-9.5;}
dwOUTval = (int)(Ana_out*4096.0/20.0 + 2048);
dwOUTval = ( dwOUTval << 4 ) & 0xfff0;
if ( (nErr = K_DAWrite(hDev1600, 0, dwOUTval)) != 0)
   {putch (7);printf("Error %X during Digital Output.",nErr);exit(1);}

// read pulse number per adj period check whether 64
DAS1600_8254GetCounter(0,0,&CtrDataL);
DAS1600_8254GetCounter(0,0,&CtrDataH);
CtrVal=(CtrDataH<<8)+CtrDataL;
pulse_number=(CtrVal_1-CtrVal)/(float)(Nadj-1);
CtrVal_1=CtrVal;


//display/write data
printf("\015");
printf("per%2dspin  N:%3.1f",Nadj,pulse_number);
printf(" Adj#:%5d  Devia:%5.0f  Avg.Current:%4.0fA  ", Cadj,Deviate,Current);

if ( (file_write3==1) && (Current>10))
        {fprintf(out3,"%d %5.0f %4.0f\n", Cadj,Deviate,Current); }

waitingADEOC:
Cadj++; time_read=0;

do
 { K_IntStatus( hFrameAD1600 , &nStatus, &dwTransfers );
        if( kbhit() )  { in_com=getch(); }

//      switch (in_com)
//      { default:break;
//        case '-':Ana_out=-5.0;in_com=0; /*manual adjust torch position*/
//                 dwOUTval = (int)(Ana_out*4096.0)/20.0 + 2048;
//                 dwOUTval = ( dwOUTval << 4 ) & 0xfff0;
//                 K_DAWrite(hDev1600, 0, dwOUTval);break;
//        case '=':Ana_out=5.0;in_com=0;
```

```
//                  dwOUTval = (int)(Ana_out*4096.0)/20.0 + 2048;
//                  dwOUTval = ( dwOUTval << 4 ) & 0xfff0;
//                  K_DAWrite(hDev1600, 0, dwOUTval);break;
//      }


   // Watch dog
   if(nStatus==2) {Cadj=-3;
                   K_IntStop(hFrameAD1600 , &nStatus, &dwTransfers);
                   goto goon;}

   gettime(&real_time);
   now_time=real_time.ti_sec+0.01*real_time.ti_hund;
   if(time_read==0) {start_time=now_time; time_read=1;}
   time_pass=now_time-start_time;
   if (time_pass<0) {time_pass+=60;}
   if( time_pass>1.0 ) { Cadj=-5;
                         K_IntStop(hFrameAD1600 , &nStatus, &dwTransfers);
                         break;}


  }while (((int)dwTransfers<Nsamp)&(in_com!='\x20'));


goon:


} while (in_com!='\x20');    //press Space bar to stop

stop:
  dwOUTval =  2048;   // stopactuator
  dwOUTval = ( dwOUTval << 4 ) & 0xfff0;
  if ( (nErr = K_DAWrite(hDev1600, 0, dwOUTval)) != 0)
    {putch (7); printf( "Error %X during Digital Output.", nErr );
        exit(1);}
  K_CloseDriver(hDrv1600) ;  //close device
  //closegraph();
  if (file_write1 == 1) { fclose(out1);}
  if (file_write2 == 1) { fclose(out2);}
```

```
  if (file_write3 == 1) { fclose(out3);}
  return 0;
} //end main

void DisplayError(char *szFuncName, short nErr)
{

  K_GetErrMsg(hDev1600, nErr, &szErrMsg);

  putch (7);
  printf("Error %X during %s operation: %Fs\n", nErr, szFuncName, szErrMsg);

}
```

B. Spinning Arc Joint Seam Tracking Codes for M68HC16 Based System (Assembly Codes)

```
******Arc Sensor EEProm program v1.0: arc1P.asm********
; Arc Sensor welding seam tracking
; For Freedom F16 V2.5 Board
; Ps at IC1, Pd at IC2, Current at Ach0
; Move to Left at PWMA, Move to Right at PWMB
; Deviation: EY<0---arc at left; EY>0---Arc at right
; Indicators at "Latch", bit 6-5-4-3(arc at left) 3-2-1-0(at right)
; bit 7: flashing @ 1/2 adjust freq. if codes running good
; EPROM: 0~3 banks, SRAM bank 4, iRAM, 4:0000~4:03ff; SFR: bank F

********** SFR names in F:XXXX

 INCLUDE    'EQU_A.F16'  ;table of EQUates for common register addresses

******Define Constant and data memory base addr.

Nresl  EQU $40      ; rotating index
Nres2  EQU Nresl*2
Nadj   EQU $5
Nfav   EQU Nadj-1
Nfsl   EQU $8
Kofst  EQU $0      ; mech.
Pofst  EQU $0      ; Phase
Ofst   EQU Kofst+Pofst

Iadr0   EQU $8000         ;at x:8000
Iadr0H  EQU $80
Ifadr0  EQU $9100         ;at x:9100
Ifadr0H Equ $91
Iffadr0 EQU $9300         ;at x:9300
Iffadr0H Equ $93
EYadr0   EQU $A000          ;at x:A000

Kp    equ $8       ; PID control parameter
Ki    equ 0
Kd    equ 0
```

```
Step0  equ $38
Step1  equ $60       ; LED control comparison points
Step2  equ $90

*****define variables at iRAM (from 0200)

Cadj   EQU $0200   ;at 4:0200
Cresl  EQU $201
Cfsl   EQU $202
Iadr   EQU $204
IadrH  EQU $204    ; this system use low byte addr store high byte of data
IadrL  Equ $205
Ifadr  EQU $206
IfadrH EQU $206
IfadrL EQU $207
Iffadr EQU $208
IffadrH EQU $208
IFFadrL EQU $209

Counter1   equ $210   ;total revolve counting
Counter2   equ $212   ; total pulse count
Counter3   equ $214   ; total adjustment count
Counter4   equ $216   ; susp. interrupt count

AdjEnab   EQU $218    ; adjusting cycle flag
iter      EQU $21A    ; general purpose iteration counter
RunLED    EQU $21C    ; keep change sign each adjusting, for flash LED

EY       equ $220
EYdata   equ $222
;EYsign   equ $224
EY_1     equ $226
EY_2     equ $228
EY_3     equ $22A
EY_4     equ $22C
Eyadr    equ $22E    ; an index reg. for recording Ey @ A000~

******fill interupt vector
INCLUDE    'VECT_1P.ASM' ;initialize reset vector to some specific
                  ;interrupt handlers. Ps: IC1 & Pd:IC2
```

```
******start the program

    ORG   $200     ;start program (this is reset addr. by VECT_1P)

***** Initialization Routines *****
Start:
INCLUDE   'INIT_1P.ASM' ;initially set EK=F, XK=4, YK=4, ZK=4
                ;set sys clock at 16.78 MHz, disable COP
                ;turn on 1k internal IRAM at $4:0000
                ;set stack in bank 4 IRAM (SK=4, SP=03FE)

*** SRAM 4:xxxx,
*** iRAM 4:0000~4:03FF, used for variables and stack
*** ROM 0:0000~3:FFFF,
*** for iRAM (variables) access, set use z offset (4:0000)
*** for SFR access EK=F : F:F000~FFFF, use Extended direct
*** Variables:  from 4:0200 up; Stack: 4:03FE down


***** Start of main program *****
main: ORP #$00E0   ; disable all interrupt: IP=111

   LDAB    #4
   TBXK       ; XK=4, YK=4, ZK=4
   TBYK
   TBZK
   LDZ     #$0000  ;z base: 4:0000, point to variables at 4:0200~

   ldd     #00     ;ppr=000,sfa/b=0:  PWM=32.8KHz (reset value)
   std     PWMC    ; PWM control reg. (reset value)
   ldaa    #$10
   staa    pwma    ; reset PWMA, PWMB
   staa    pwmb
   ldab    #%01110111
   stab    Latch

**** INitiate Timer,IC,OC
   LDD     #$008E  ;
   STD     GPTMCR  ; set GPT IARB=0E
```

```
    LDD     #$0440   ; GPT IRQ level 4, vector 64
    STD     GPTICR   ; IPA=0000,no adj on prio. IPL=4, level 4
             ; IVBA=$40, i.e GTP_vector start at #64 vector
    LDAB #%00000000 ; disable OC,IC
    STAB TMSK1
    LDAB #$06    ; time base: system/256
    STAB TMSK2   ;
    LDAB #%00000101; IC1, IC2 rising, others disabled
    STAB TCTL2

**** Initiate A/D
    ldaa #%00000000 ; set a/d configure to awake and no freeze
    staa adcmcr ;
    ldd #%0000000010000100 ; 10bit, speed 1/10 clock
    std adctl0 ;

**** Initiate varoables
    Clr Cadj,z
    Clr Cresl,z
    Clr Cfsl,z
    Clr AdjEnab,z
    LDAA #$FF
    STAA RunLED,z
    ClrW Counter1,z
    ClrW Counter2,z
    ClrW Counter3,z
    ClrW counter4,z

    ldd #$3000
    std iter,z
    LDY #Iadr0       ; clr $8000~AFFF
ClrMem:clrw 0,y
    AIY  #2
    decw iter,z
    decw iter,z
    BGT ClrMem

    Ldaa #Iadr0H     ; #$80
    Staa IadrH,z
    Ldaa #Ifadr0H    ; #$91
```

```
    Staa IfadrH,z
    Ldaa #Iffadr0H     ; #$93
    Staa IffadrH,z
    LDD  #EYadr0       ; #$A000
    STD  Eyadr,z

****Set Watchdog
    LDAA #$B0 ; 1 0 11 0 0 00: Enable watchdog, 512*2^15*/fsys (16.7Mhz)
              ; disable halt monitor, fsys=512*fref=512*32.768KHz
              ; disable bus to ext monitor, 64 S_clk timeout bus monitor
    STAA SYPCR    ; $B0 enables the watchdog (COP) for 1 sec timeout
    ldaa #$55     ; write/start watchdog
    staa SWSR
    ldaa #$AA
    staa SWSR

    LDAB #%00000001 ; enable IC1 interrupt
    STAB TMSK1
    BCLR TFLG1,#1   ; clr IC1 pending bit
    ORP  #$0070   ;enable interrupt level 4 (Ps) and higher, IP=011*
    ANDP #$FF7F

MainLP:
    BRCLR AdjEnab,z,#$F0,mainlp   ;loop here except adjust time

PreAdj: LDAB #%00000000  ; disable GPT (IC1) interrupt
    STAB TMSK1
    LDD #$00B0        ; disable Int level 5 and lower
    TDP
    LBSR Adjust
PostAdj:Ldaa #$0F
    STAA AdjEnab,z   ; clear adj enable flag
    LDAB #%00000001  ; set IC1 interrupt only
    STAB TMSK1
    LDD  #$0070      ; enable Int level 4 and up
    TDP
    BRA mainlp

*******Ps Interrupt process*******
```

```
PsISR:
    LDAB #%00000000 ; disable IC1,IC2 interrupt
    STAB TMSK1
    BCLR TFLG1,#1   ; clr IC1 pending bit
    Clr  Cresl,z    ; clear rotation position to 0,
    Incw Counter1,z
    Inc  Cadj,z
    LDAA Cadj,z     ;
    CMPA #Nadj
    BLT  Readab
adjab:          ; if Cadj>=Nadj, this cycle adjust
    Ldaa #$F0
    STAA AdjEnab,z  ; Cadj: 0,1,2,3,4-0-1, 2,3,4-0-1,
    Clr Cadj,z
    RTI

Readab:         ; this cycle read data
    Clr  Cresl,z

    LDAA Cadj,z   ; high byte of Iadr. (need plus Dmbase: 80)
    ADDA #Iadr0H  ; #$80  result A: 81,82,83,84, for Nadj=5
    Ldab #Ofst    ; e.g. #Ofst=7
    ROLB        ; double it (lower byte of Iadr.: 0E)
    STD  Iadr,z   ; I first addr. at first circle: 810E
    LDAA #Ifadr0H ; #$91, If first addr. (high byte of Ifadr)
    STD  Ifadr,z  ; Lower byte same as Iadr: 910E

    Bclr TFLG1,#3   ; clear IC2 pending
    LDAB #%00000011 ; enable IC1,IC2 interrupt
    STAB TMSK1
    RTI

*******Pd Interrupt Service*****
PdISR:
    Bclr TFLG1,#2   ; clear IC2 pending
    incw Counter2,z
    ldd #$0       ; trigger A/D, single 4-conv single chan: 0
    std adctl1 ;

    Ldab IadrL,z
```

```
    CMPB #Nres2-2
    BLS PdLB1
    CLR IadrL,z  ;
    CLR IfadrL,z ; IY=
PdLb1:LDY Iadr,z    ; (Iadr) sent to Y

adwait:NOP
    BRCLR adstat,#$1,adwait ;
    lde  rjurr0   ; read Adresult: right justified UNSIGNED,
StoreAD:ste  0,y     ; Iadr0=0000, Ofst=7,
              ; final addr: 810E for 1st circle, 1st point

*** average ****
    ClrE
    ldaa #Nfav
    staa iter,z
    LDAA #Iadr0H   ; #$80
    LDAB IfadrL,z
PdLB2:INCA       ; high byte of current data addr.: (Cadj+iter)mode Nfav
    XGDY       ; (A:B) sent to y, but A byte changed
    ADDE 0,y    ; sum I of same HighByte addr.; 10bit*max16cycle=<14bit
    XGDY       ; resume D from Y
    dec iter,z
    BGT PdLB2   ; iter>0 add more, =0, Nfav number added, finish

    TED        ; sent sum to LowWord (max14bit: 10bit AD *max16cycle)
    ClrE       ; clear High Word
    Ldx  #Nfav
    Ediv       ; UNsigned (E:D)/ix, Accum/Nfav=avarege at ix; 10bit
    LDY Ifadr,z ;
AvgEnd: STX  0,y    ; UNSIGNED result sent to If memory

****average end

*****closing Pd****
    INC IadrL,z ; next I addr.
    INC IadrL,z
    INC IfadrL,z ; next If addr.
    INC IfadrL,z
    INC Cresl,z ; for counting only
```

```
    RTI

*******Subroutine, Data process: Adjust*****
Adjust:
    incw Counter3,z

    ldaa #$55     ; write watchdog
    staa SWSR
    ldaa #$AA
    staa SWSR

***copy If to lower end ***

    LDY #Ifadr0
    LDD #Ifadr0
    SUBD #Nres2
    xgdx        ;lower end If base addr.
    ldaa #Nresl
    Staa iter,z
    LDE #2
SldLB1:LDD 0,y     ; copy If to x
    STD 0,x
    AEX
    AEY
    dec iter,z
    BGT SldLB1    ; copy Nresl data. when A=0 finished

***Copy If to higher end ***
    LDY #Ifadr0
    TYX
    AIX  #Nres2   ; (higher end copy starting addr.)
    ldaa #Nresl
    staa iter,z
    LDE #2
AdjLB1:
    LDD 0,y
    STD 0,x      ; copy If to x
    AEX
    AEY
    dec iter,z
```

```
    BGT AdjLB1   ; copy Nresl data. when A=0 finished

***sliding average***  may change to use MAC

    LDD #Ifadr0
    STD Ifadr,z      ;source data If starting addr.
    LDD #Iffadr0
    STD Iffadr,z     ;dest. data Iff starting addr.
    LDAA #Nresl
    STAA Cresl,z
AdjLB3:        ;loop repeat Nresl times, for each point in a revolve
    LDE  Ifadr,z
    sube #Nfsl*2 ; first source data If addr. at each sliding window
    xgey      ;  iy: source

    LDAA #Nfsl*2+1
    STAA Cfsl,z
    CLRD
AdjLB2:ADDD 0,y    ;repeat Nfsl times; 10bit*max17point=<15bit
    Aiy #2
    dec Cfsl,z
    BGT AdjLB2
          ; sum at D LowWord (max14bit: 10bit AD *max16cycle)
    ClrE      ; clear High Word
    Ldx  #Nfsl*2+1
    Ediv      ; Unsigned, (E:D)/ix, sum/Nfsl=avarege (10bit) at ix
    LDY Iffadr,z
    STX  0,y    ; average UNSIGNED result sent to Iff memory
          ; Can also thought as SIGEND (as always positive) int or fra.

    incw Iffadr,z
    incw Iffadr,z
    incw Ifadr,z
    incw Ifadr,z
    DEC Cresl,z
    BGT AdjLB3
SldEnd: NOP
***sliding average end***

*******compute error EY****: EY=Right-Left
```

```
; EY >0: torch on right; EY < 0: torch at left of groove

    LDX  #Iffadr0  ; data Iff base addr.;low 10 bit effective, Signed posi.
    LDY  #COStab   ; COStab base addr   ; 16bit full Signed
    LDHI
    CLRD
    TDMSK
    LDE  #Nresl-1
    CLRM
    RMAC 2,2     ; IX,IY step up 2 byte each iteration
    TMXED        ; AM[31:0] sent to E:D, ; 32 bit signed fraction
            ; max: 64*16bit*10bit=32bit
    TED
    STD  EY,z    ; deviation value with sign

    ldy  EYadr,z ;record all Ey @ RAM A000~FFFF
    STD  0,y
    incw Eyadr,z
    incw Eyadr,z
    bmi  goon1
    ldd  #EYadr0
    std  Eyadr,z
goon1: nop

CalEnd: STD  EYdata,z ; D may not be positive
    BGE  NCgSign
CGSgin:NEGD
    STD  EYdata,z ; if Neg, make positive
NCgSign:NOP

**** end computing Ey***

*****Feedback control and output to indicator****
    CLRB
    STAB PWMA
    STAB PWMB

    LDD EYdata,z
    LDE #Kp
    EMUL
```

```
    TSTE
    BEQ MVLB1
    LDD #$FFFF   ;saturate D

MVLB1:TSTW EY,z   ; + Right high; - left high
    Bmi MtoR

****** Arc At right, Move TO LEFT  (Ey>0)******

MtoL:STAA PWMA    ; pin pwmA: move to Left

***output to LED: latch bit (3)-2-1-0
    CMPA #Step0
    BHI R123     ; R level 1/2/3
Cen1: Ldab #%00001000 ; R very small
    BRA Adjout
R123:  CMPA #Step1
    BHI R23      ; R level 2/3
R1:  LDAB #%00001100
    BRA Adjout
R23:   CMPA #Step2
    BHI R3
R2:  LdaB #%00001110
    BRA Adjout
R3:  Ldab #%00001111
    BRA Adjout

*****Arc At Left, Move TO RIGHT ( Ey<0 )

MToR: STAA PWMB    ; pin PWMB : move to Right

***Show arc position, output to LED: "latch"  bit 6-5-4-(3)
    CMPA #Step0
    BHI L123     ; L level 1/2/3
Cen2: Ldab #%00001000 ; L very small
    BRA Adjout
L123: CMPA #Step1
    BHI L23      ; L level 2/3
L1:  LDAB #%00011000
    BRA Adjout
```

```
L23:  CMPA #Step2
      BHI L3
L2:   LdaB #%00111000
      BRA Adjout
L3:   Ldab #%01111000
      BRA Adjout

Adjout:
      EORB #%11111111     ; NOT B, latch use sink circuit, B.7=1
      NEG RunLED,z
      BMI  KeepB7         ; RunLED change sign each adjusting
NotB7: EORB #%10000000    ; NOT B.7 only
KeepB7:STAB latch

****Clear If zone;  if Pd lost there will no further adj (all If & Iff=0)
      LDY #Ifadr0   ; 9100 zone
      LDAA #$40
clrIf:Clrw 0,y
      AIY #2
      deca
      bne clrIf

      BCLR TFLG1,#1      ; clr IC1 pending bit
      RTS

******END OF PROCESSING SUBroutine********

******All other no-use interrupt services
NoCare: incw counter4,z
      RTI

******fill a data table at high end of "ROM"

      ORG $3F00
COStab:    ; cos(i/64*2Pi)*32768  (i=0,1,...64, 16 bit signed fraction)

      dw $7FFF,$7F62,$7D8A,$7A7D,$7642,$70E3,$6A6E,$62F2    ; 0~90 degree
      dw $5A82,$5134,$471D,$3C57,$30FC,$2528,$18F9,$0C8B

      dw $0000,$F375,$E707,$DAD8,$CF04,$C3A9,$B8E3,$AECC    ; 90~180
```

```
dw $A57E,$9D0E,$9592,$8F1D,$89BE,$8583,$8276,$809E

dw $8001,$809E,$8276,$8583,$89BE,$8F1D,$9592,$9D0E    ; 180~270
dw $A57E,$AECC,$B8E3,$C3A9,$CF04,$DAD8,$E707,$F375

dw $0000,$0C8B,$18F9,$2528,$30FC,$3C57,$471D,$5134    ; 270~360
dw $5A82,$62F2,$6A6E,$70E3,$7642,$7A7D,$7D8A,$7F62; $7FFF
```